Supplementary information

Imaging-Guided Companion Diagnostics in Radiotherapy by Monitoring APE1 Activity with Afterglow and MRI Imaging

Renye Yue[1,2], Zhe Li[1], Huiyi Liu[1], Youjuan Wang[1], Yuhang Li[3], Rui Yi[1], Baoli Yin[1], Haisheng Qian[2], Heemin Kang[4,5], Xiaobing Zhang[1], Guosheng Song[1,5*]

[1] State Key Laboratory of Chemo/Biosensing and Chemometrics, College of Chemistry and Chemical Engineering, Hunan University Changsha 410082 (P.R. China)

[2] School of Biomedical Engineering, Research and Engineering Center of Biomedical Materials, Anhui Medical University, Hefei 230032 (P.R. China)

[3] Department of Hepatobiliary Surgery/Central Laboratory, Hunan Provincial People's Hospital (The First Affiliated Hospital of Hunan Normal University), Changsha 410082 (P.R. China)

[4] Department of Materials Science and Engineering and College of Medicine, Korea University, Seoul 02841(Republic of Korea)

[5] Shenzhen Research Institute, Hunan University, Shenzhen 518000, China

*Corresponding author

E-mail address: Song G (songgs@hnu.edu.cn)

Contents

Supplementary Figures

Supplementary Tables

Supplementary References

Supplementary Figures

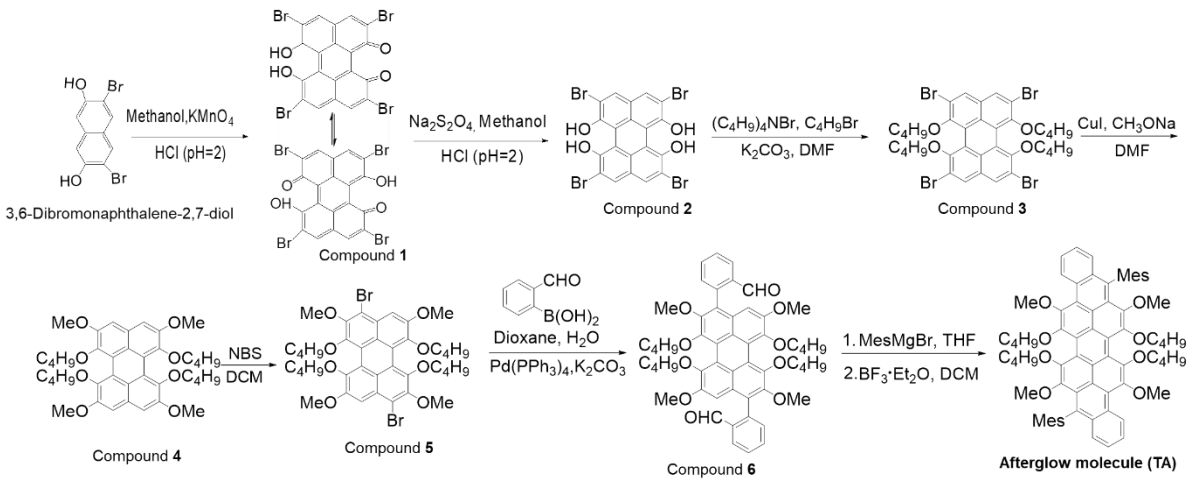

Supplementary Fig. 1 The synthesis procedure for TA molecules[1,2].

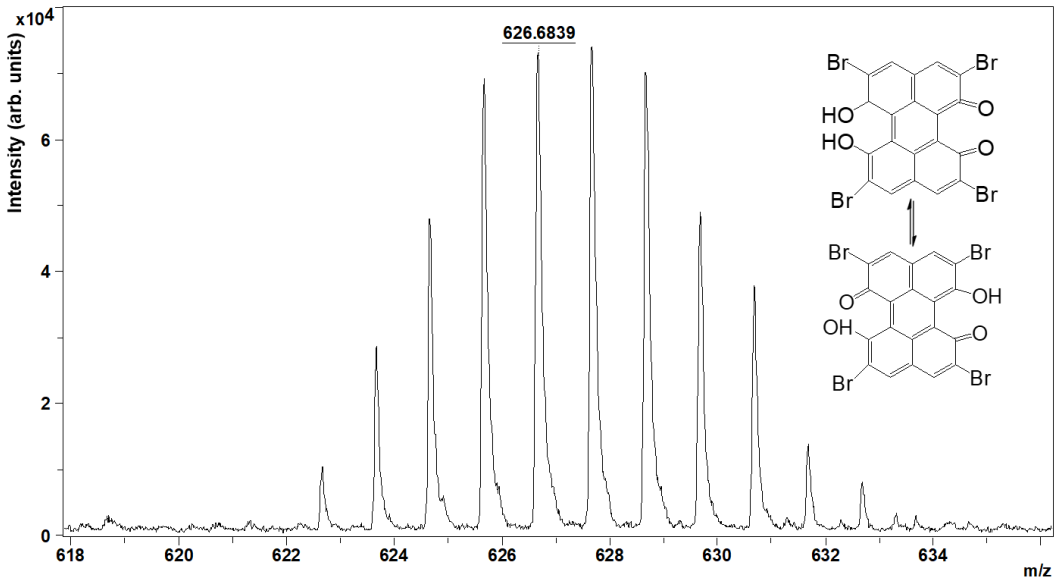

Supplementary Fig. 2 HR (MALDI-TOF) mass spectrum of Compound **1**.

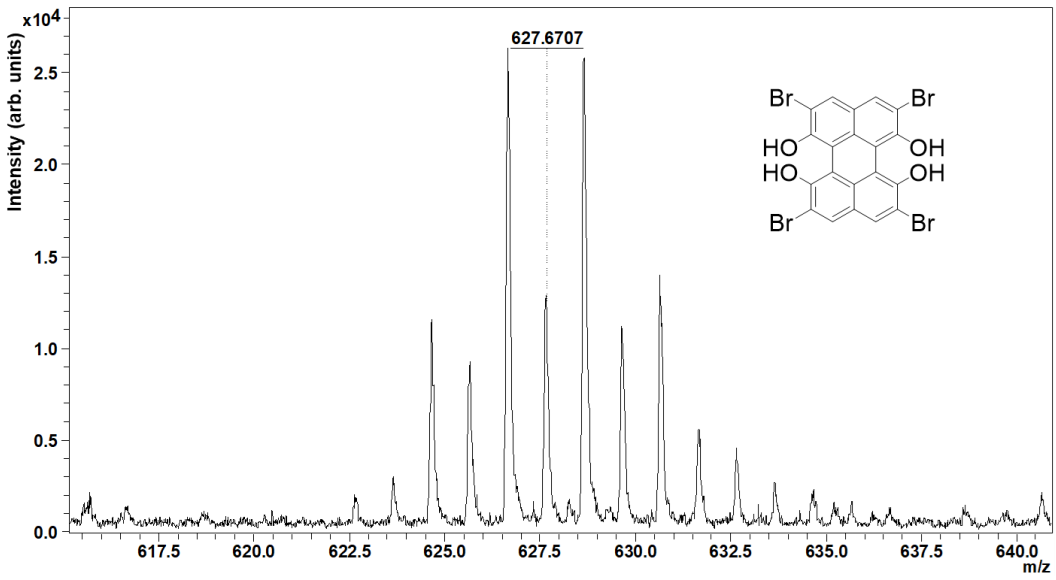

Supplementary Fig. 3 HR (MALDI-TOF) mass spectrum of Compound **2**.

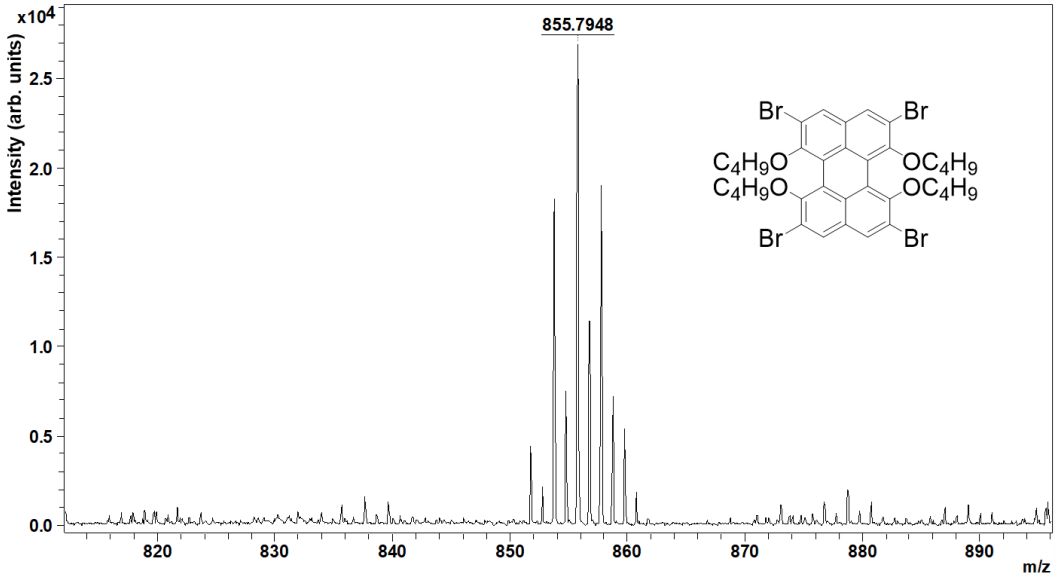

Supplementary Fig. 4 HR (MALDI-TOF) mass spectrum of Compound **3**.

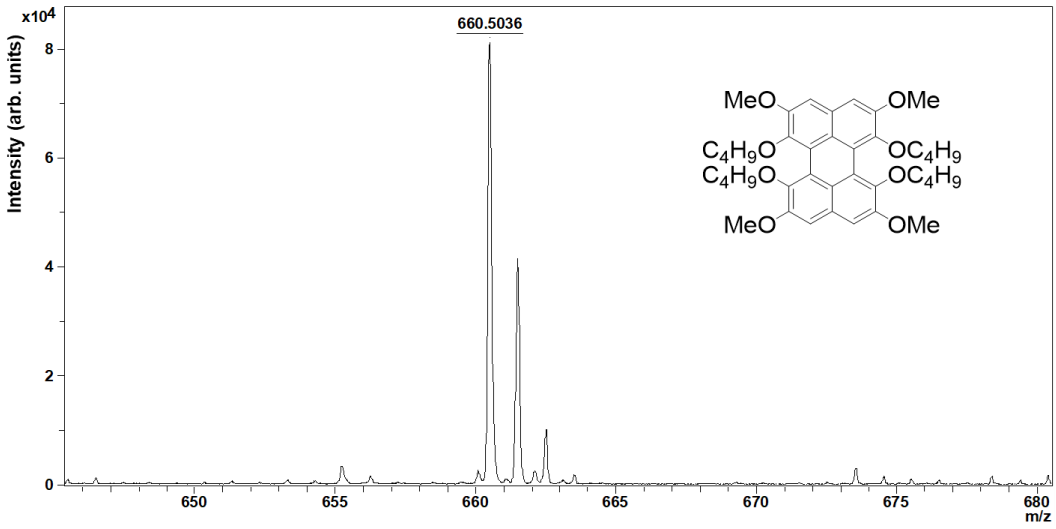

Supplementary Fig. 5 HR (MALDI-TOF) mass spectrum of Compound **4**.

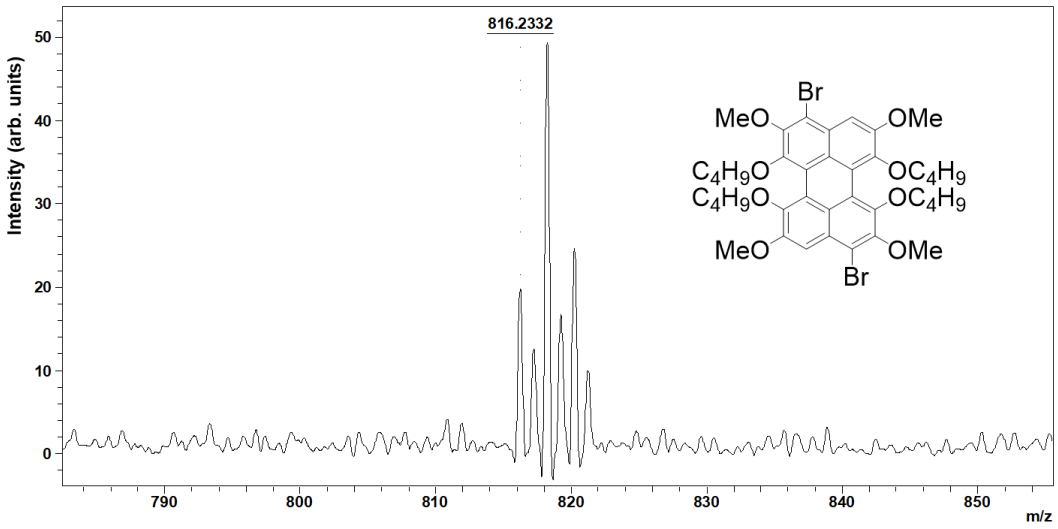

Supplementary Fig. 6 HR (MALDI-TOF) mass spectrum of Compound **5**.

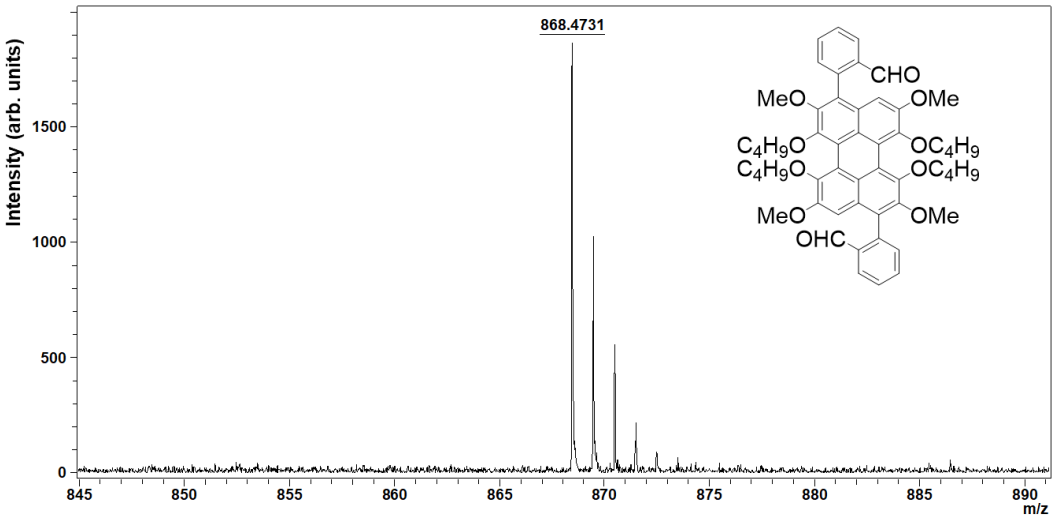

Supplementary Fig. 7 HR (MALDI-TOF) mass spectrum of Compound **6**.

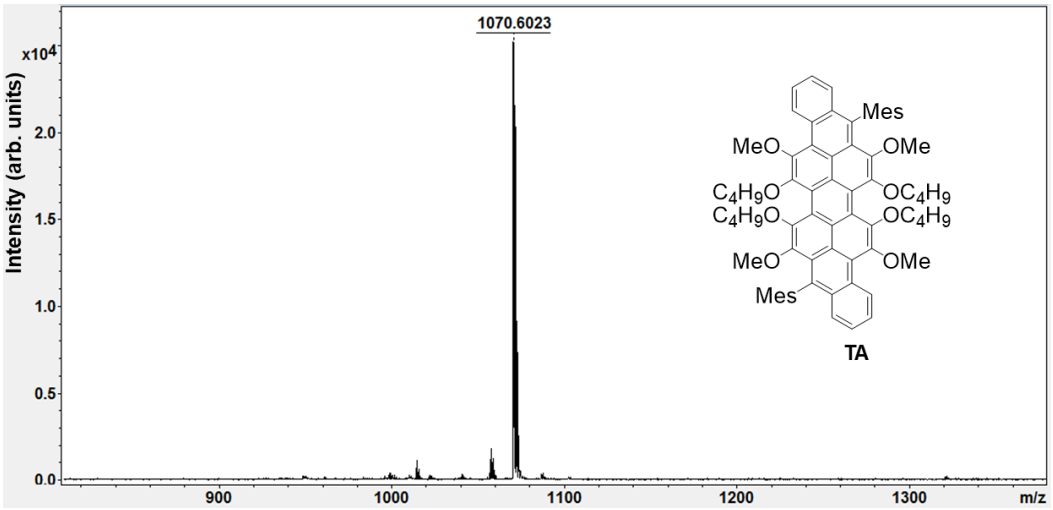

Supplementary Fig. 8 HR (MALDI-TOF) mass spectrum of afterglow molecules (TA).

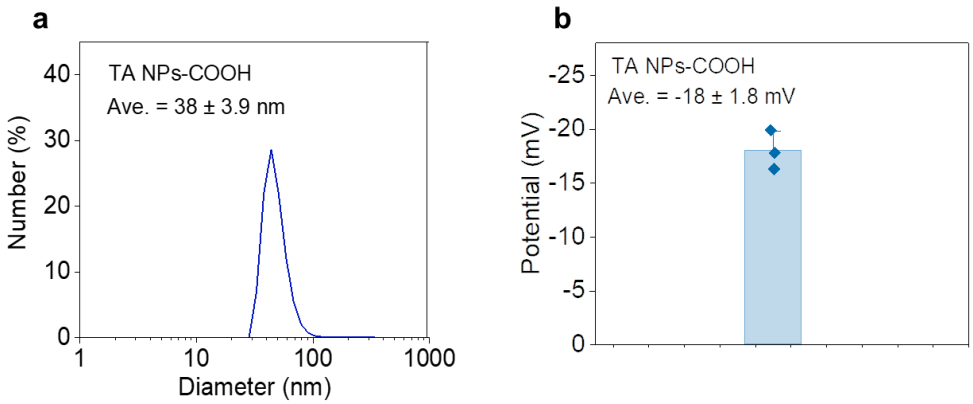

Supplementary Fig. 9 Characterization of afterglow nanoparticles (TA NPs). (a) Representative DLS measurement at water condition (n = 5 independent experiments). (b) Zeta potential (n = 3 independent experiments). Data are presented as means ± SD.

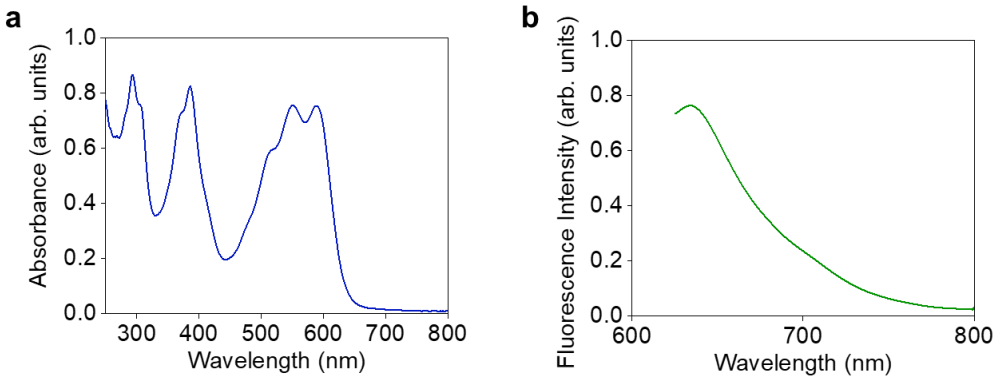

Supplementary Fig. 10 Optical characterization of TA NPs (n = 3 independent experiments). (a) Representative absorption spectrum. (b) Representative fluorescence spectrum.

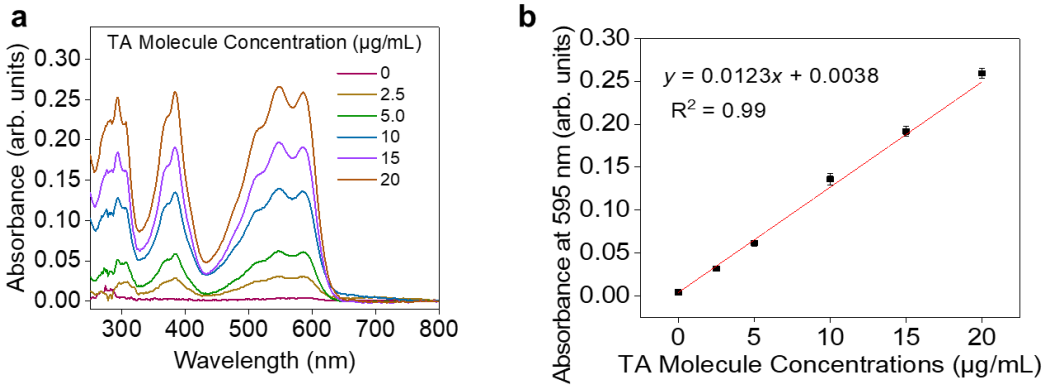

Supplementary Fig. 11 Determination of TA NP concentrations. (a) Absorbance spectra of TA+PFODBT dye under various concentrations. (b) Standard curve for quantification analysis of TA NP concentration (n = 3 independent experiments). Data are presented as means ± SD.

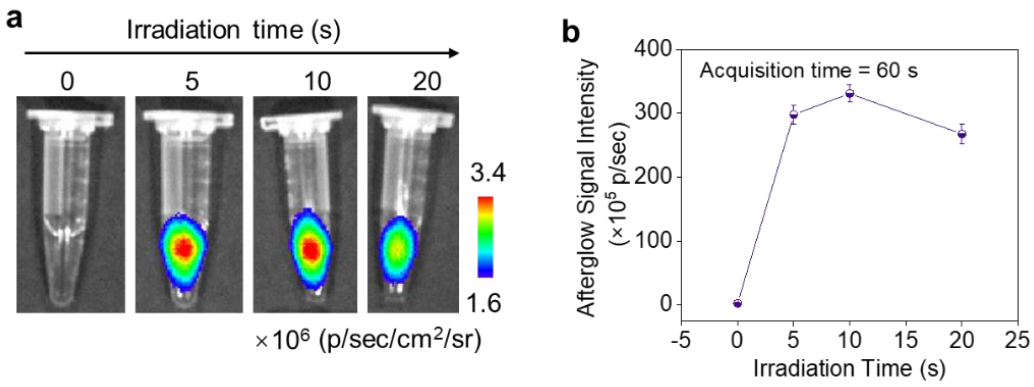

Supplementary Fig. 12 Afterglow characterization of TA NPs (20 μg/mL) under various times of irradiation under a fixed acquisition time of 60 s (10 mW/cm^2, n = 3 independent experiments). (a) Representative afterglow images. (b) Quantified afterglow signal intensity from (a). Data are presented as means ± SD.

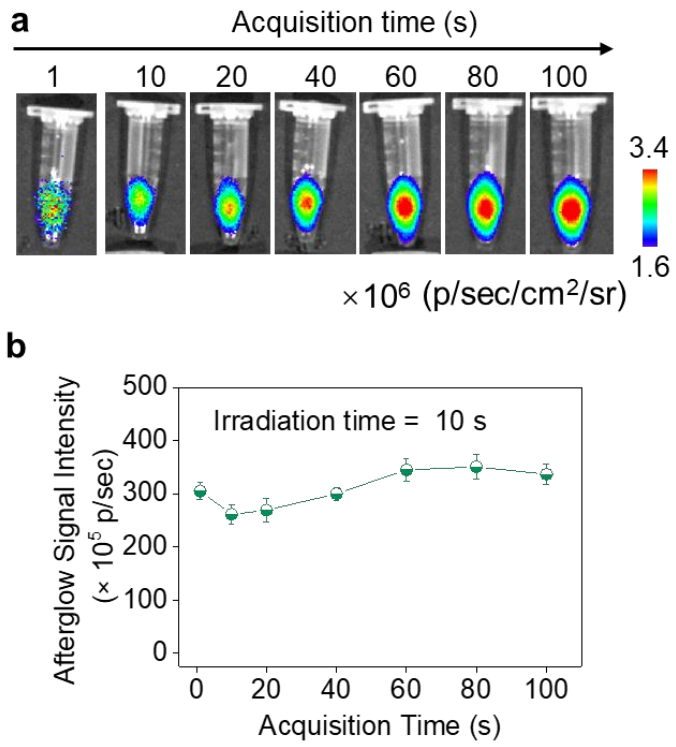

Supplementary Fig. 13 Afterglow characterization of TA NPs (20 μg/mL) with various acquisition times under a fixed irradiation time of 10 s (10 mW/cm^2, n = 3 independent experiments). (a) Representative afterglow images. (b) Quantified afterglow signal intensity from (a). Data are presented as means ± SD.

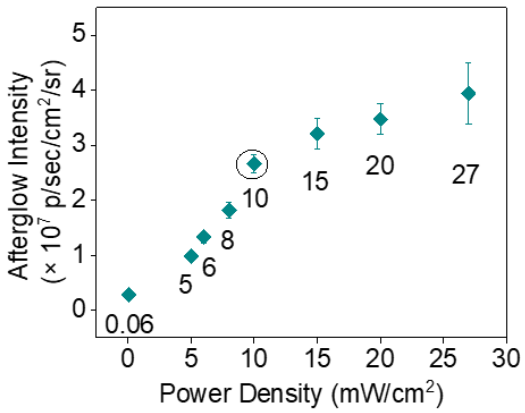

Supplementary Fig. 14 Afterglow luminescence signal intensity of TA NPs (20 μg/mL) under different-power density irradiation (irradiation time: 10 s, acquisition time: 60 s, n = 6 independent experiments). Data are presented as means ± SD.

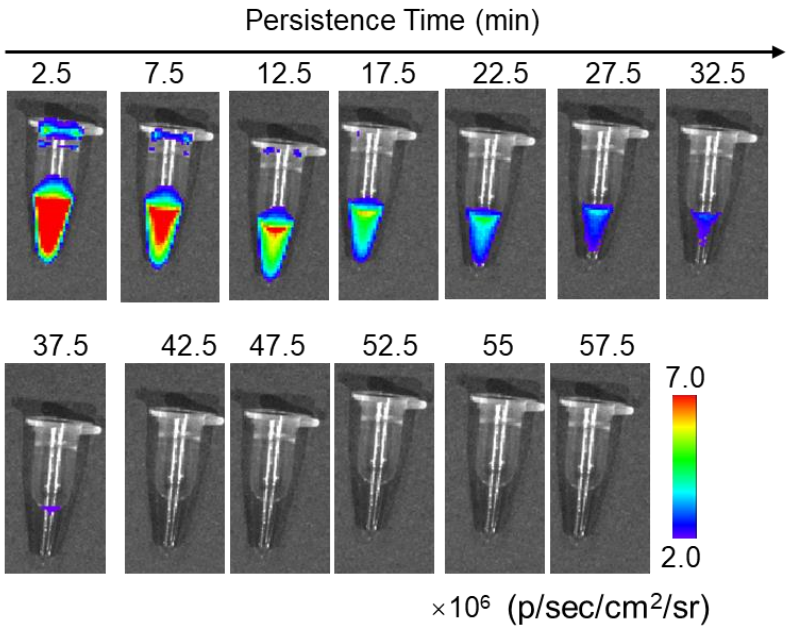

Supplementary Fig. 15 Representative afterglow images for testing signal attenuation of TA NPs (30 μg/mL, 10 mW/cm^2, irradiation time: 10 s, acquisition time: 60 s, n = 3 independent experiments).

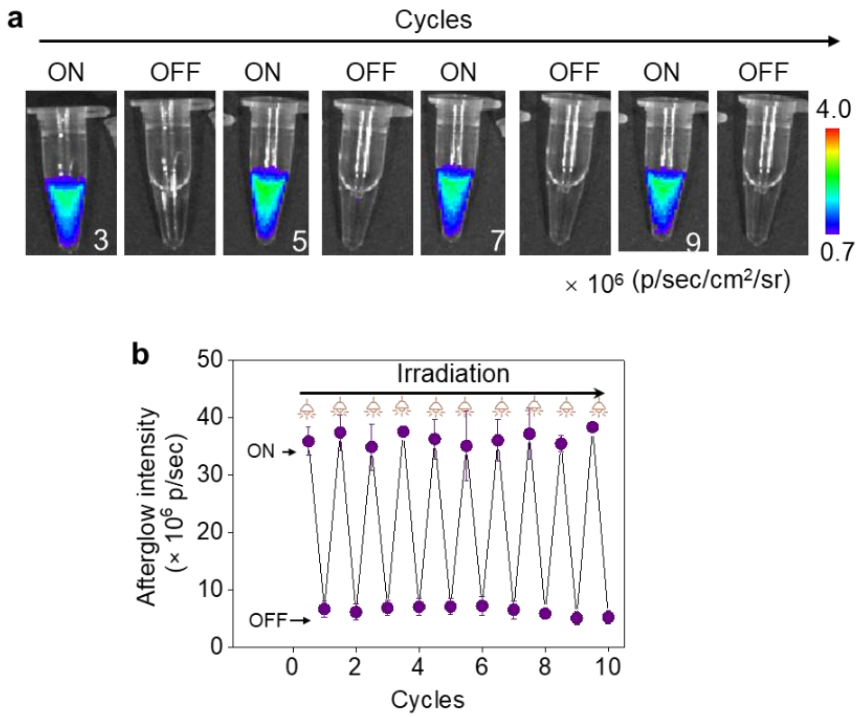

Supplementary Fig. 16 Afterglow imaging of TA NPs under 10-recycle recharge (30 μg/mL, 10 mW/cm^2, irradiation time: 10 s, acquisition time: 60 s, n = 6 independent experiments). (a) Afterglow images. (b) Quantified afterglow signal intensity. Data are presented as means ± SD.

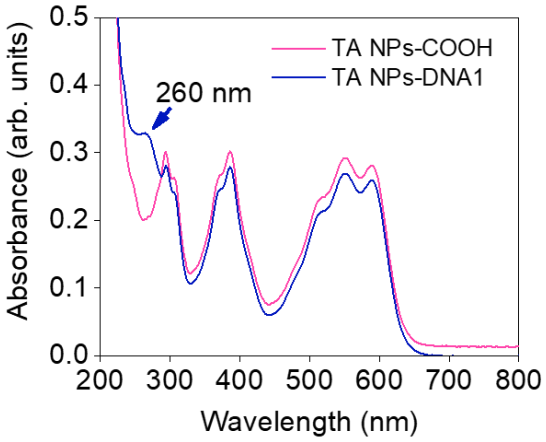

Supplementary Fig. 17 Representative Absorption spectra of TA NPs before and after conjugating with DNA1 (n = 3 independent experiments).

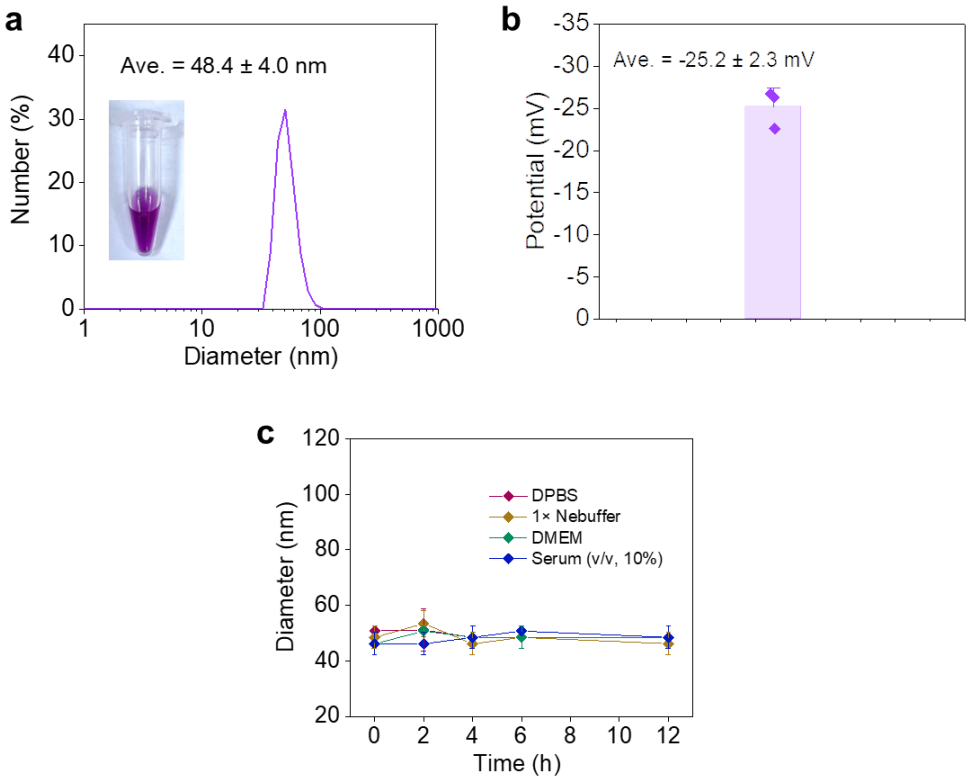

Supplementary Fig. 18 Characterization of TA NPs-DNA1. (a) DLS measurement at water condition (Insert: photograph image, 50 μg/mL TA NPs) (n = 3 independent experiments). (b) Zeta potential (n = 3 independent experiments). (c) DLS measurement of TA NPs-DNA1 under different conditions (DPBS, 1×NeBuffer, DMEM, and serum (V_{serum}: V_{H2O} = 1: 9), respectively) for 0, 2, 4, 6, 12 hours (n = 3 independent experiments). Data are presented as means ± SD.

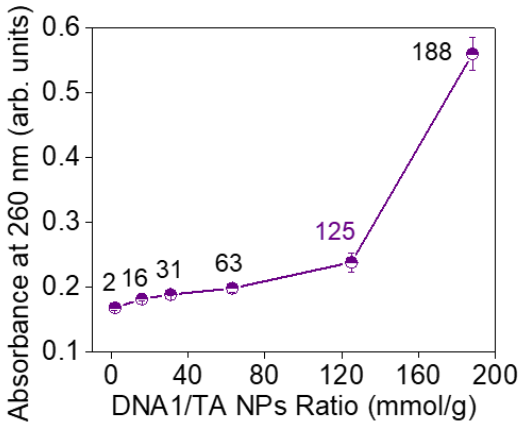

Supplementary Fig. 19 Absorbance determination of free DNA1 from TA NPs-DNA1 solution under various modification ratios of DNA1 and TA NPs (n = 3 independent experiments). Data are presented as means ± SD.

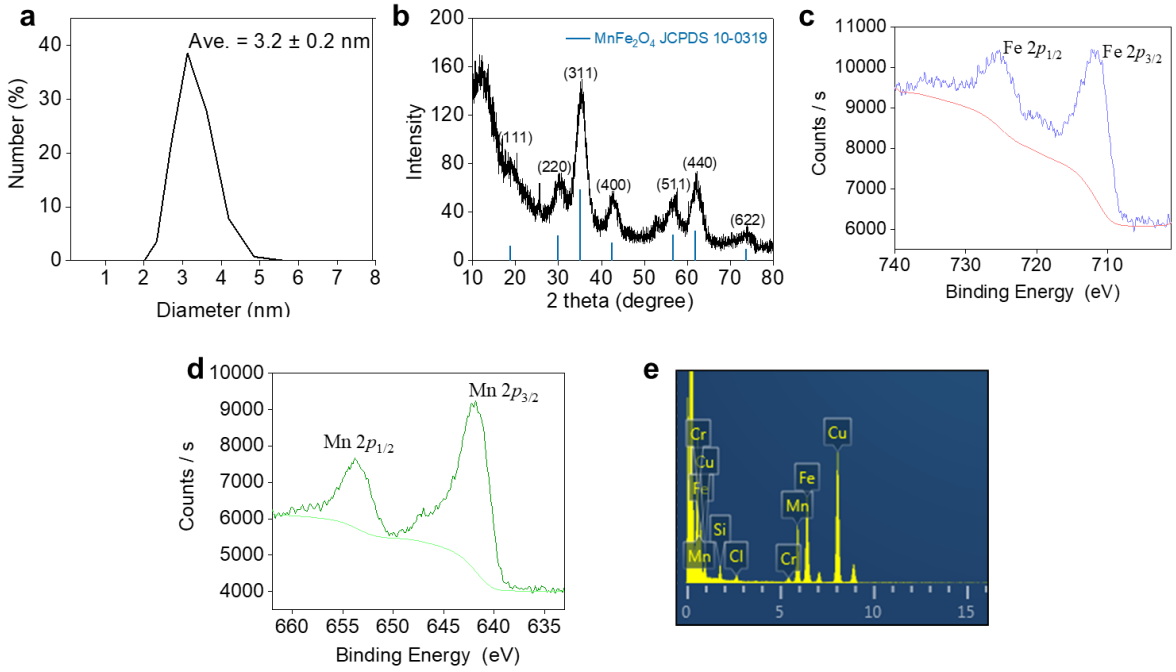

Supplementary Fig. 20 Characterization of $FeMnO_x$ nanoparticle. (a) DLS determination of $FeMnO_x$-OA at chloroform condition (n = 4 independent experiments). Data are means ± SD. (b) Powder X-ray diffraction (*XRD*) patterns of the $FeMnO_x$ nanoparticle. (c and d) Fe 2*p* and Mn 2*p* X-ray photoelectron spectroscopy (*XPS*) of the $FeMnO_x$. (e) Energy dispersive X-ray analysis of $FeMnO_x$.

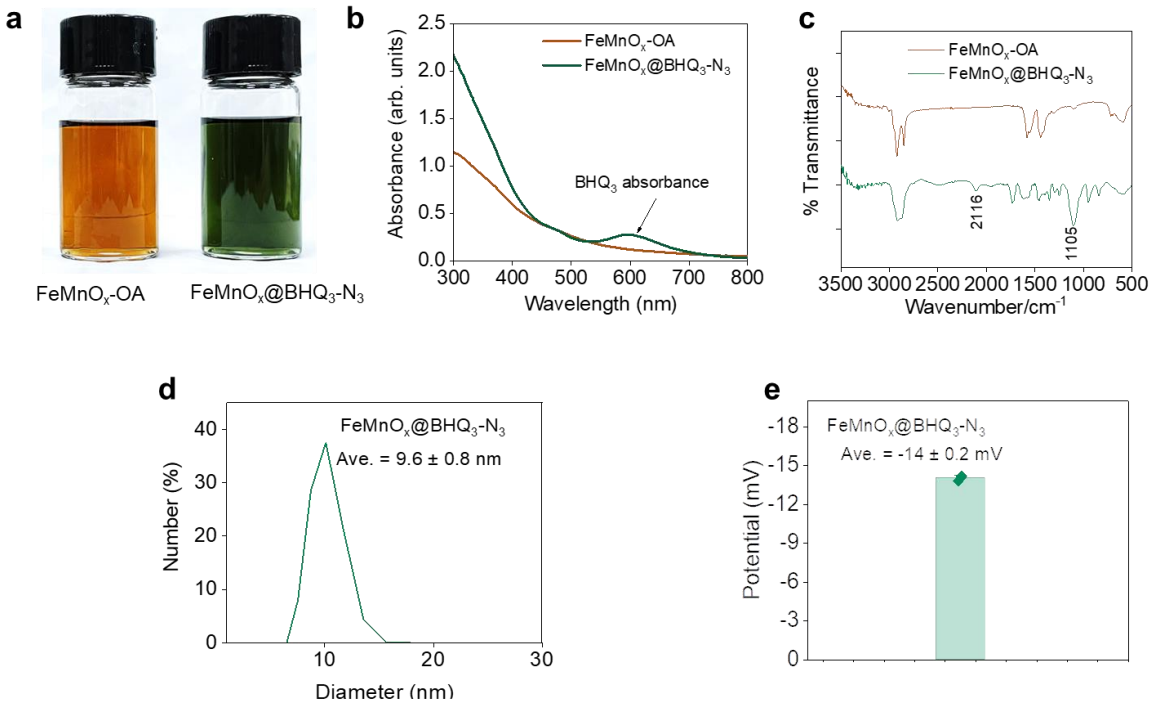

Supplementary Fig. 21 Characterization of $FeMnO_x$@BHQ_3-N_3. (a) Photographs images of $FeMnO_x$ (containing 0.31 mg/mL, Fe + Mn) before and after conjugating with NH_2-BHQ_3 and p-PEG-N_3. (b) Representative absorbance spectra of $FeMnO_x$ and $FeMnO_x$@BHQ_3-N_3. (c) *FT-IR* spectra of $FeMnO_x$ and $FeMnO_x$@BHQ_3-N_3. (d) Representative DLS measurement at water condition (n = 3 independent experiments). (e) Zeta potential (n = 3 independent experiments). Data are presented as means ± SD.

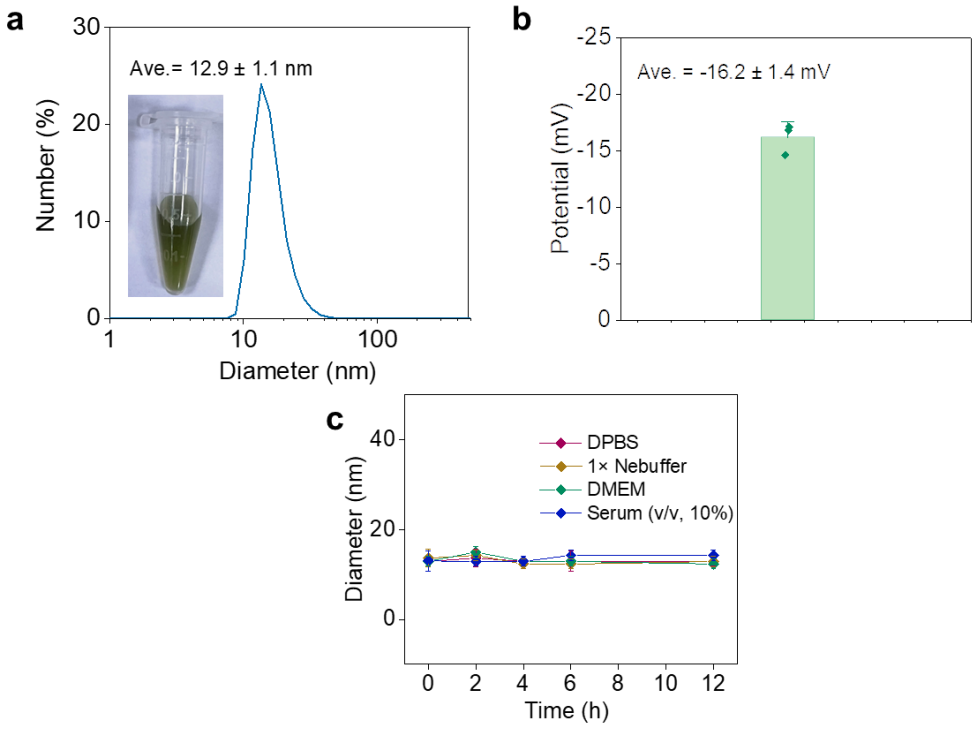

Supplementary Fig. 22 Characterization of $FeMnO_x$ conjugation with DNA2 ($FeMnO_x$-DNA2). (a) Representative DLS measurement (Insert: photograph images, 0.25 mg/mL, Fe + Mn) (n = 3 independent experiments). (b) Zeta potential (n = 3 independent experiments). (c) DLS measurement of $FeMnO_x$-DNA2 under different conditions (DPBS, 1×NeBuffer, DMEM, and serum (V_{serum}: V_{H2O} = 1: 9), respectively for 0, 2, 4, 6, 12 hours (n = 3 independent experiments). Data are presented as means ± SD.

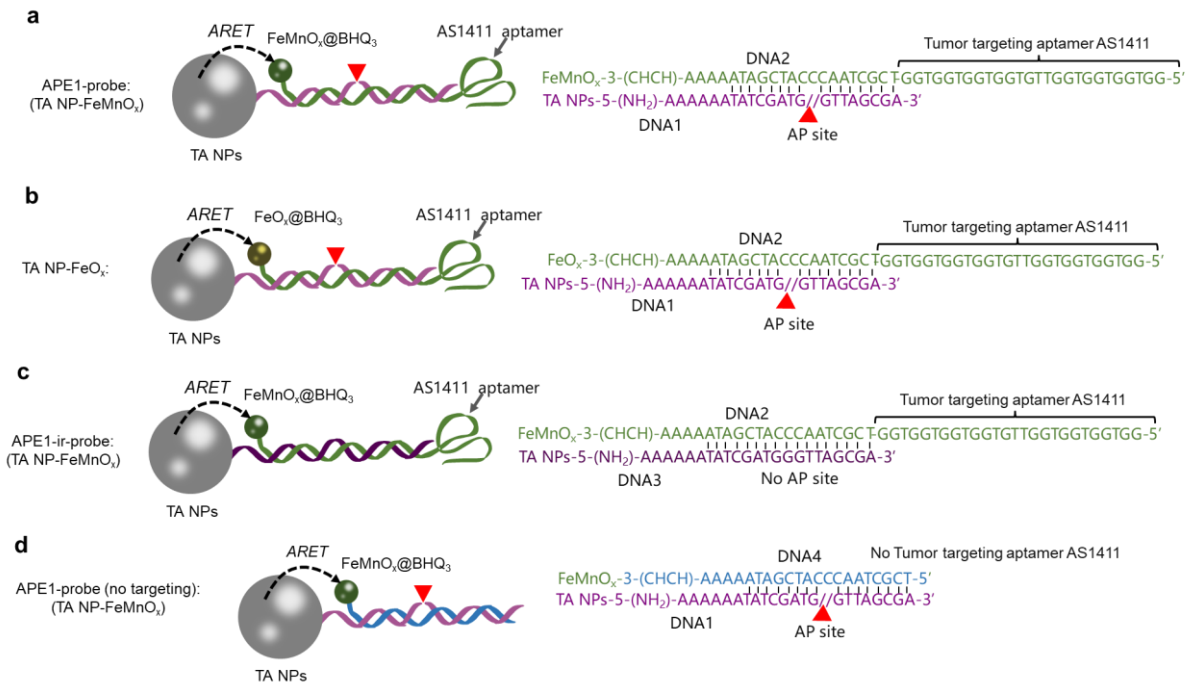

Supplementary Fig. 23 Schematic illustration for the structures and DNA sequence of various probes. (a) TA NP-$FeMnO_x$ (APE1-probe). (b) TA NP-FeO_x. (c) APE1-irresponsive probe (APE1-ir-probe, no AP site). (d) APE1-probe (no targeting aptamer).

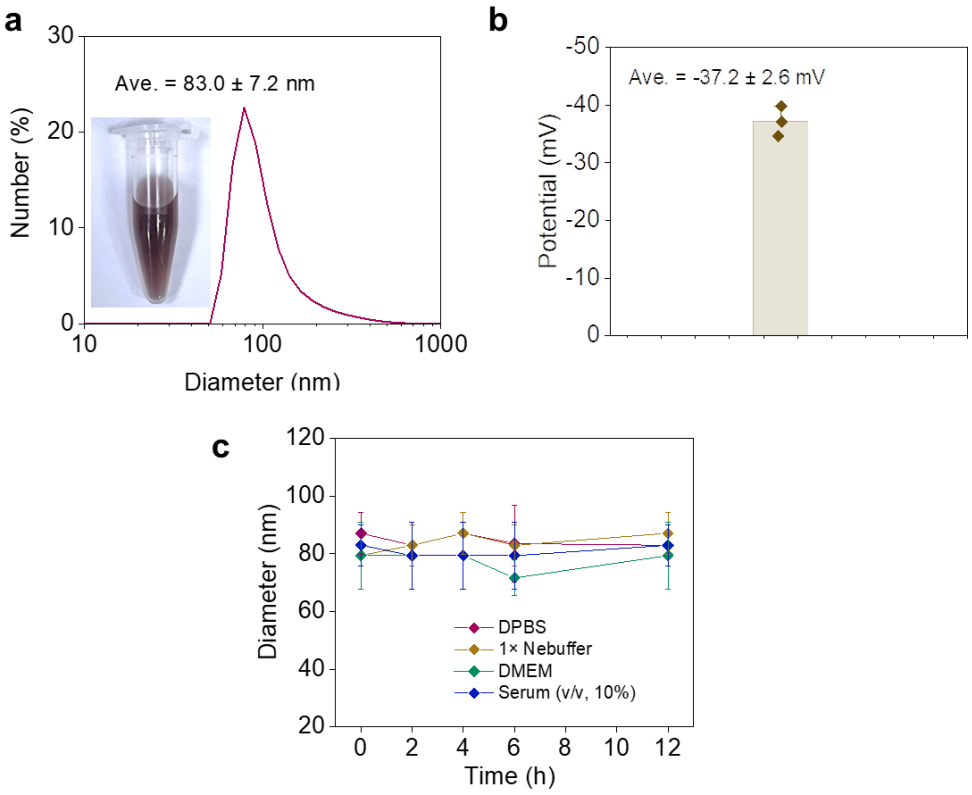

Supplementary Fig. 24 Characterization of TA NPs-DNA1 and $FeMnO_x$-DNA2 assembly (APE1-probe). (a) Representative DLS measurement (Insert: photograph image, containing 50 μg/mL TA NPs) in DPBS (n = 3 independent experiments). (b) Zeta potential (n = 3 independent experiments). (c) DLS measurement of APE1-probe under different conditions (DPBS, 1×NeBuffer, DMEM, and serum (V_{serum}: V_{H2O} = 1: 9), respectively for 0, 2, 4, 6, 12 hours (n = 3 independent experiments). Data are presented as means ± SD.

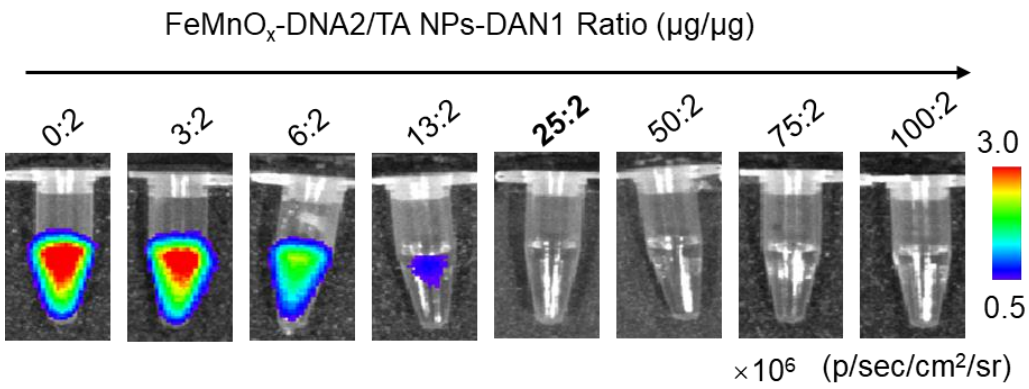

Supplementary Fig. 25 Afterglow images of TA NPs-DNA1 (10 μg/mL) assembling with various ratios of $FeMnO_x$-DNA2 (10 mW/cm^2, irradiation time: 10 s, acquisition time: 60 s, n = 3 independent experiments).

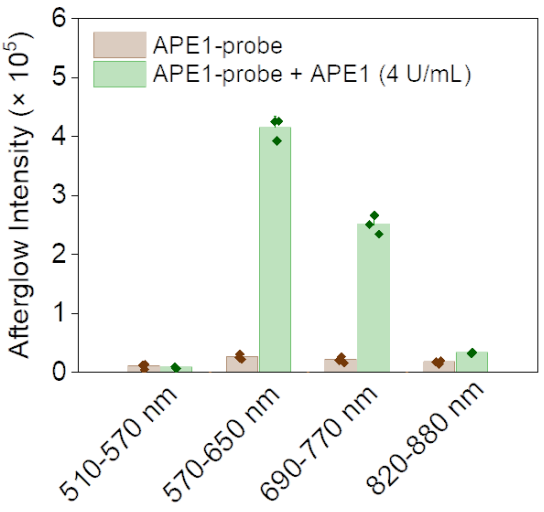

Supplementary Fig. 26 The different emission channels of afterglow signal intensity of APE1-probe (5 μg/mL) before and after APE1 activation in different channels. The afterglow imaging of the samples using the IVIS spectrum imaging system (Lumina XR) (10 mW/cm^2, irradiation time: 10 s, acquisition time: 60 s, n = 3 independent experiments). Data are presented as means ± SD.

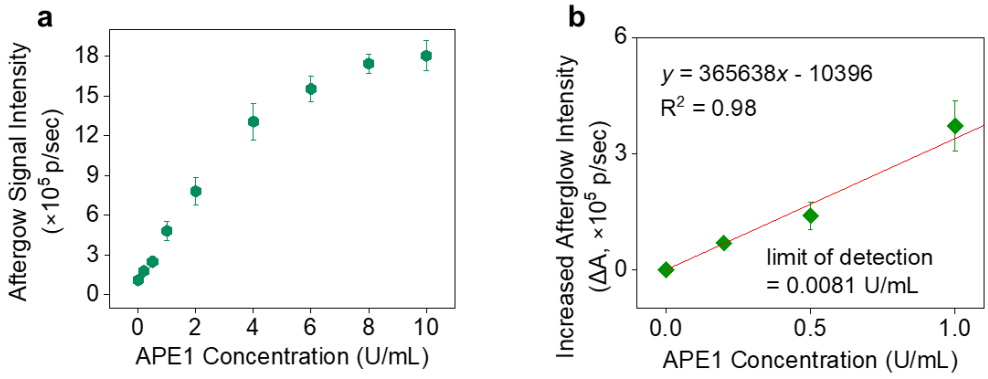

Supplementary Fig. 27 Afterglow imaging of APE1-probe (5 μg/mL) after incubating with various concentrations of APE1 (0 – 10 U/mL) in 1 × Nebuffer (10 mW/cm^2, irradiation time: 10 s, acquisition time: 60 s, n = 6 independent experiments). (a) Afterglow signal intensity. (b) A near-liner curve between the afterglow signal and APE1 concentration (0 – 1 U/mL). Data are presented as means ± SD.

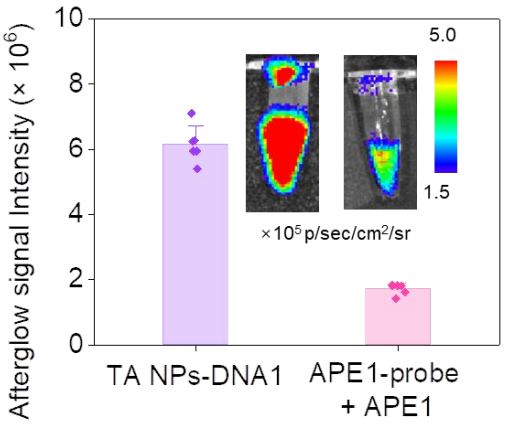

Supplementary Fig. 28 The afterglow luminescence intensities of TA NPs -DNA1 (5 μg/mL) and APE1-probe incubated with APE1 (4 U/mL) in 1 × Nebuffer (10 mW/cm^2, irradiation time: 10 s, acquisition time: 60 s, n = 6 independent experiments), as well as the data of recovery rate of APE1-probe after incubation with APE1 (recovery rate = 28.0 ± 2.0%). Data are presented as means ± SD.

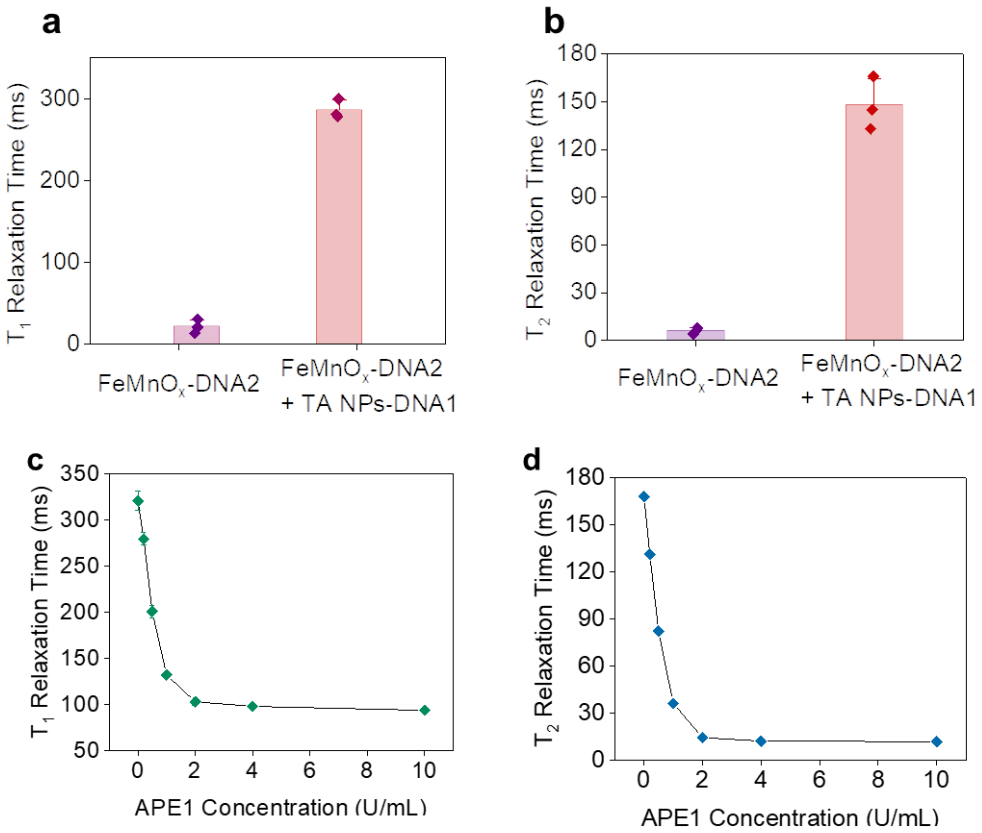

Supplementary Fig. 29 Relaxation time determination. (a) T_1 relaxation time and (b) T_2 relaxation time of FeMnO$_x$-DNA2 (20.8 μL, 0.3 mg/mL) and FeMnO$_x$-DNA2 (20.8 μL, 0.3 mg/mL) assembling with TA NPs-DNA1(100 μL, 5 μg/mL). (c) T_1 relaxation time and (d) T_2 relaxation time of APE1-probe (5 μg/mL) after incubating with various concentrations of APE1 (0 – 10 U/mL) (n = 3 independent experiments). Data are presented as means ± SD.

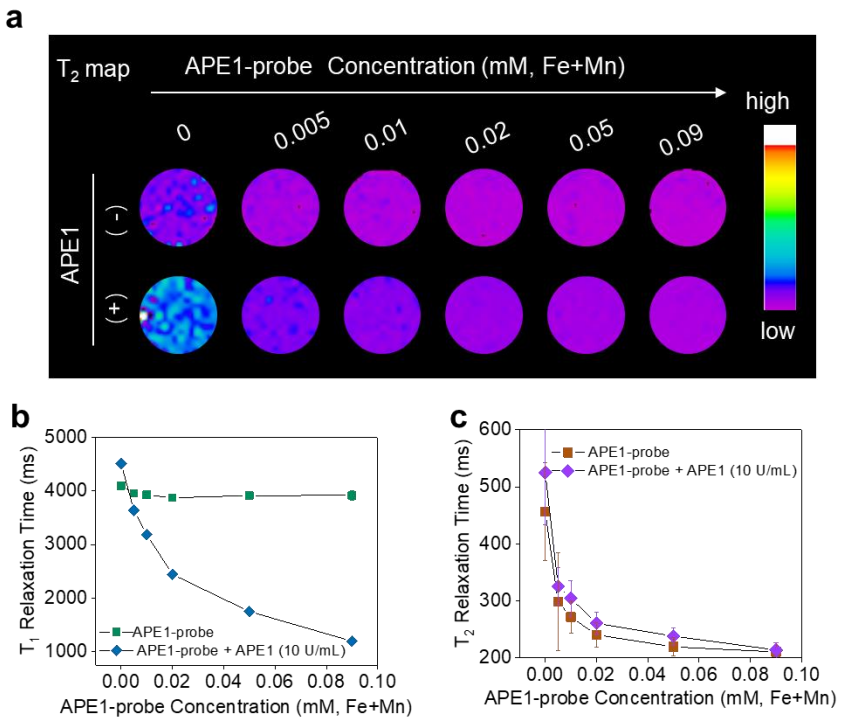

Supplementary Fig. 30 Relaxation time mapping determination of different concentrations of APE1-probe before or after APE1 incubation (n = 3 independent experiments). (a) T_2 mapping images. (b) Quantified of T_1 relaxation time. (c) Quantified of T_2 relaxation time. Data are presented as means ± SD.

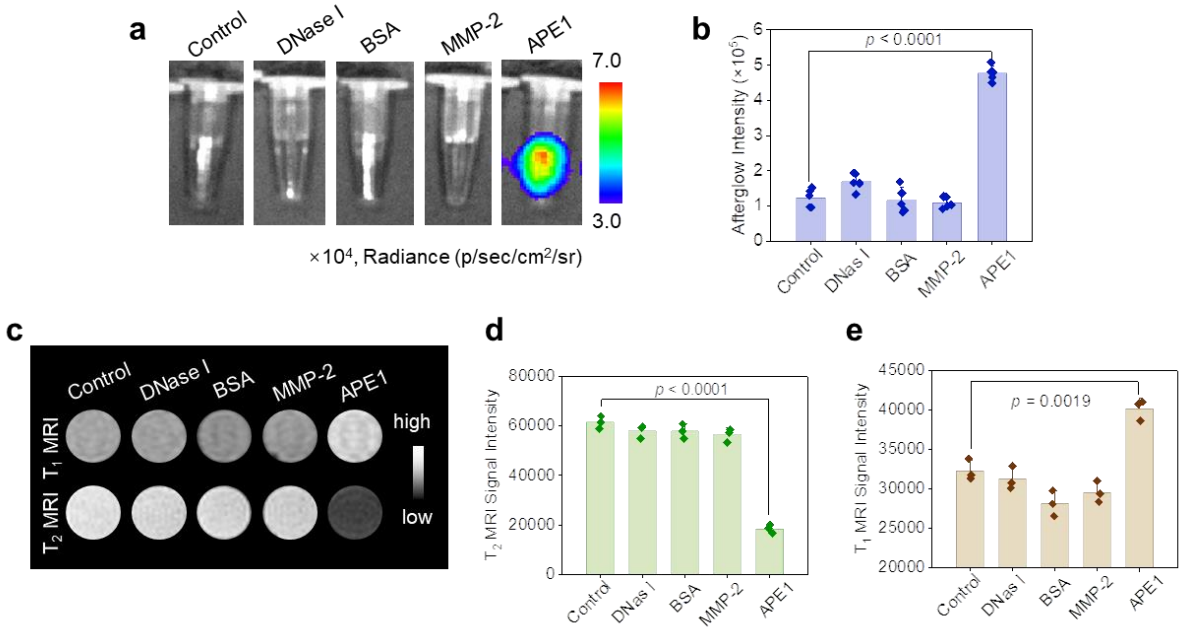

Supplementary Fig. 31 Specific determination of APE1-activated APE1-probe. (a and b) Afterglow images and quantified signal intensity of APE1-probe (containing 2 μg/mL TA NPs) incubated with DNase I (5 U/mL), BSA (500 ng/mL), MMP-2 (500 ng/mL), and APE1 (4 U/mL), respectively (10 mW/cm^2, irradiation time: 10 s, acquisition time: 60 s, n = 6 independent experiments). (c) T_1 and T_2 MRI images of APE1-probe (4 μg/mL) incubated with DNase I (5 U/mL), BSA (500 ng/mL), MMP-2 (500 ng/mL), and APE1 (4 U/mL), respectively (n = 3 independent experiments). (d and e) Quantification of T_1 and T_2 MRI signal intensity from (c). Data are presented as means ± SD. Statistical significance was determined using a two-tailed Student's t-test for pairwise comparisons, and a one-way ANOVA analysis of variance for multiple groups. P values > 0.05 were considered non-significant, while p values < 0.05 were considered statistically significant.

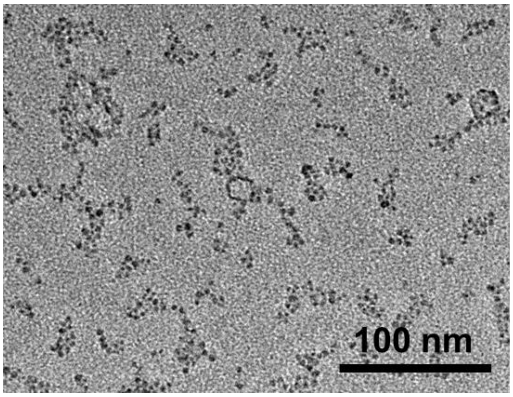

Supplementary Fig. 32 Representative TEM image of ultrasmall iron oxide nanoparticle (FeO_x).

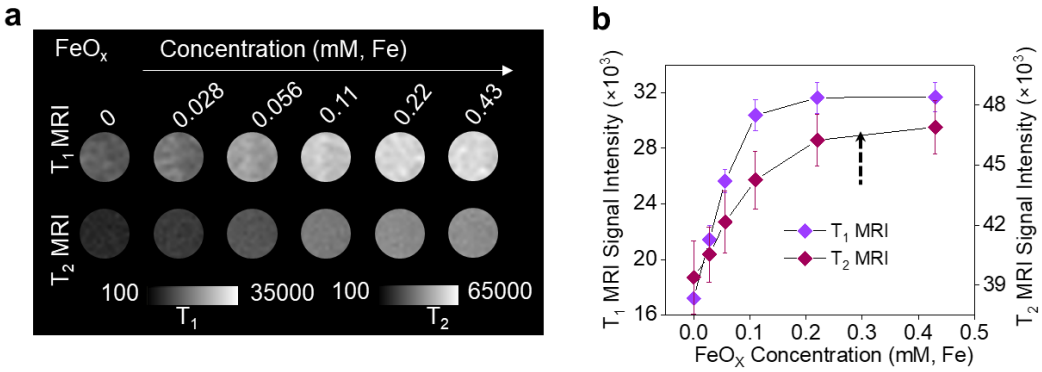

Supplementary Fig. 33 Representative MRI determination of different concentrations of FeO_x@BHQ_3-N_3 nanoparticle (n = 3 independent experiments). (a) T_1 and T_2 images. (b) Quantified of MRI signal Intensity from(a). Data are presented as means ± SD.

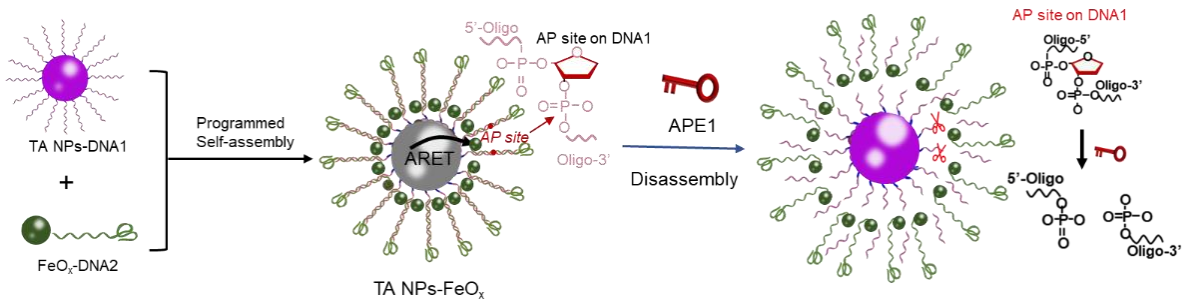

Supplementary Fig. 34 Schematic illustration for preparation and response process of APE1-activated TA NPs-FeO_x disassembly.

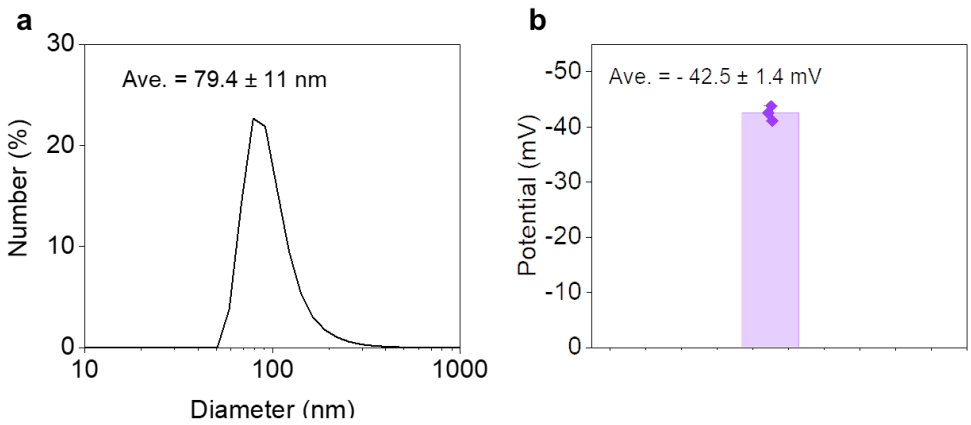

Supplementary Fig. 35 Characterization of APE1-ir-probe (the assembly of TA NPs-DNA3 and $FeMnO_x$-DNA2. (a) Representative DLS measurement at water condition (n = 3 independent biological samples). (b) Zeta potential (n = 3 independent experiments). Data are presented as means ± SD.

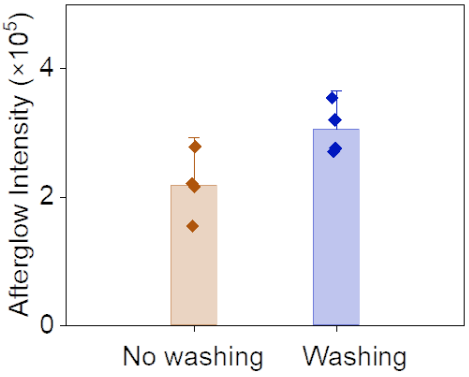

Supplementary Fig. 36 Afterglow imaging comparison of APE1-probe-incubated HeLa cells before and after washing. HeLa cells were treated with radiation (6 Gray). After 2 hours, those treated cells were incubated with APE1-probe for 4 hours. The cells were collected after DPBS washing for afterglow imaging (10 mW/cm^2, irradiation time: 10 s, acquisition time: 60 s, n = 4 independent biological samples). The cells were collected without DPBS washing for afterglow imaging and were used as the controls. The signals presented are corrected values. Data are presented as means ± SD.

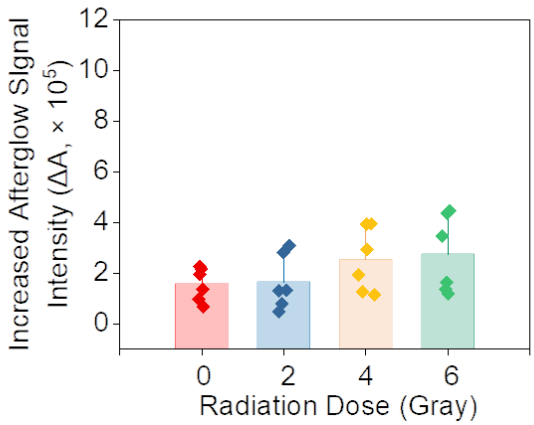

Supplementary Fig. 37 Afterglow intensity of HEK293 cell (1 ×10^7 cell/mL) incubated with APE1-probe (10 μg/mL) for 4 hours after radiation treatment (0, 2, 4, and 6 Gray, respectively) (10 mW/cm^2, irradiation time: 10 s, acquisition time of 60 s, n = 6 independent biological samples after DPBS washing). Data are presented as means ± SD.

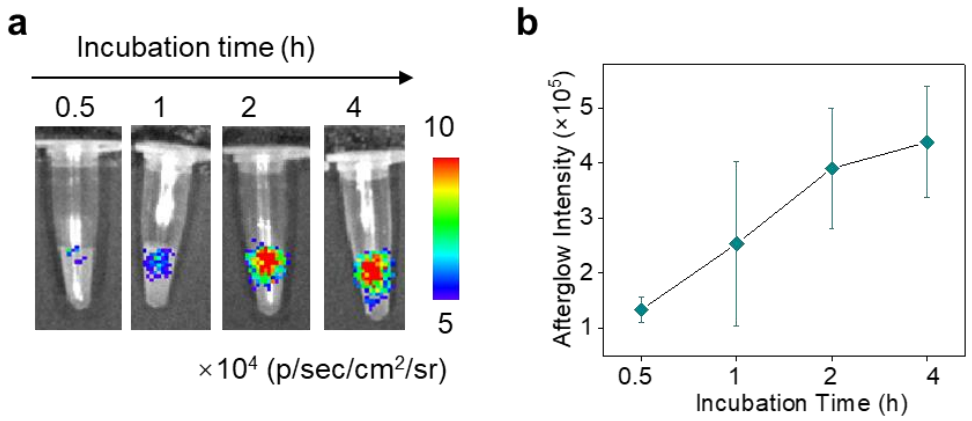

Supplementary Fig. 38 Afterglow imaging and quantification of the HeLa cell after incubating with APE1-probe for various times (after radiation of 6 Gray) (10 mW/cm^2, irradiation time: 10 s, acquisition time: 60 s, n = 6 independent biological samples after DPBS washing). (a) Afterglow images. (b) Quantification of afterglow signal intensity from (a). Data are presented as means ± SD.

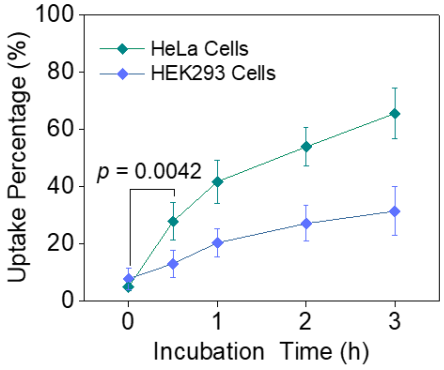

Supplementary Fig. 39 Quantification of uptake percentage of APE1-probe into two types of cells (HeLa and HEK293 cells) after radiation (6 Gray) (10 mW/cm^2, irradiation time: 10 s, acquisition time: 60 s, n = 3 independent biological samples after DPBS washing). Data are presented as means ± SD. Statistical significance was determined using a two-tailed Student's t-test for pairwise comparisons, and a one-way ANOVA analysis of variance for multiple groups. P values > 0.05 were considered non-significant, while p values < 0.05 were considered statistically significant. HeLa cells and HEK293 cells were seeded into a 48-well plate for 24 hours, and then the cells were treated with 6 Gray of radiation. After 2 hours, the treated cells were incubated with APE1-probe (containing 10 μg/mL TA NPs) at various times. The cells from different times were collected, counted, and diluted for Inductively Coupled Plasma Mass Spectrometry (ICP-MS) measurement.

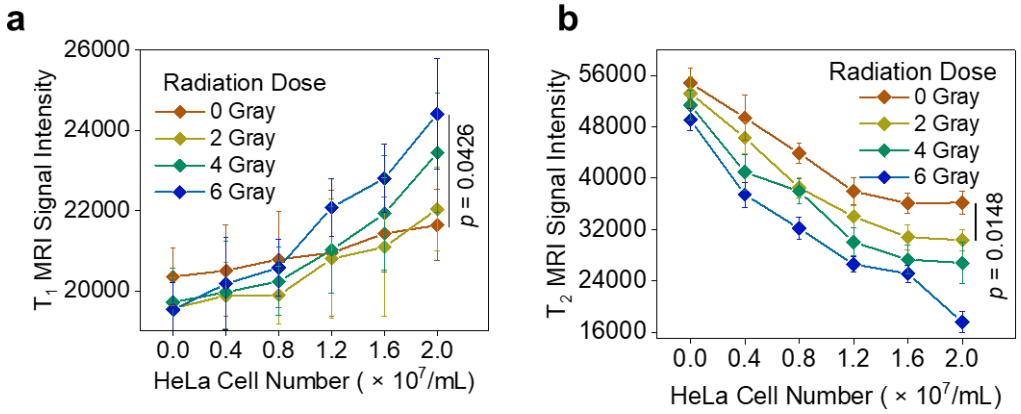

Supplementary Fig. 40 MRI signal intensity of the various concentrations of HeLa cells treated with various doses of radiation (0, 2, 4, and 6 Gray, respectively) and APE1-probe (n = 3 independent biologically samples after DPBS washing). (a) Quantified T_1 MRI signal intensity. (b) Quantified T_2 MRI signal intensity. Data are presented as means ± SD. Statistical significance was determined using two-tailed Student's t-test for pairwise comparisons, and one-way ANOVA analysis of variance for multiple groups. P values > 0.05 were considered non-significant, while p values < 0.05 were considered statistically significant.

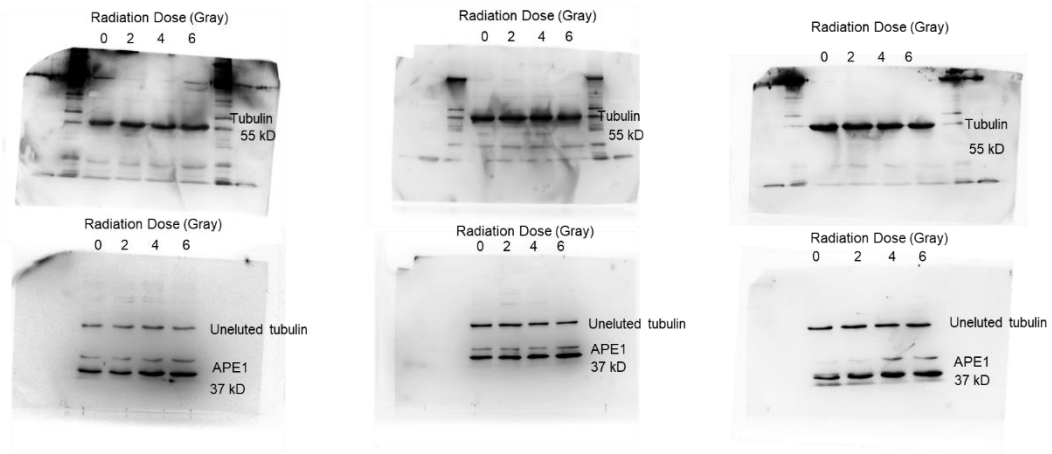

Supplementary Fig. 41 Uncropped western blot images depicting the levels of APE1 (37 kDa) and the intrinsic reference protein tubulin (55 kDa) in HeLa cells following a post-treatment period of 2 hours under varying radiation doses. The images, captured with an exposure time of 15 seconds, clearly show the distinct bands corresponding to the protein levels after treatments with 0, 2, 4, and 6 Gray, respectively, from left to right. These images are captured using the Tanon 4600 Chemiluminescent Imaging system (Tanon, China) and exported image is the format of TIFF.

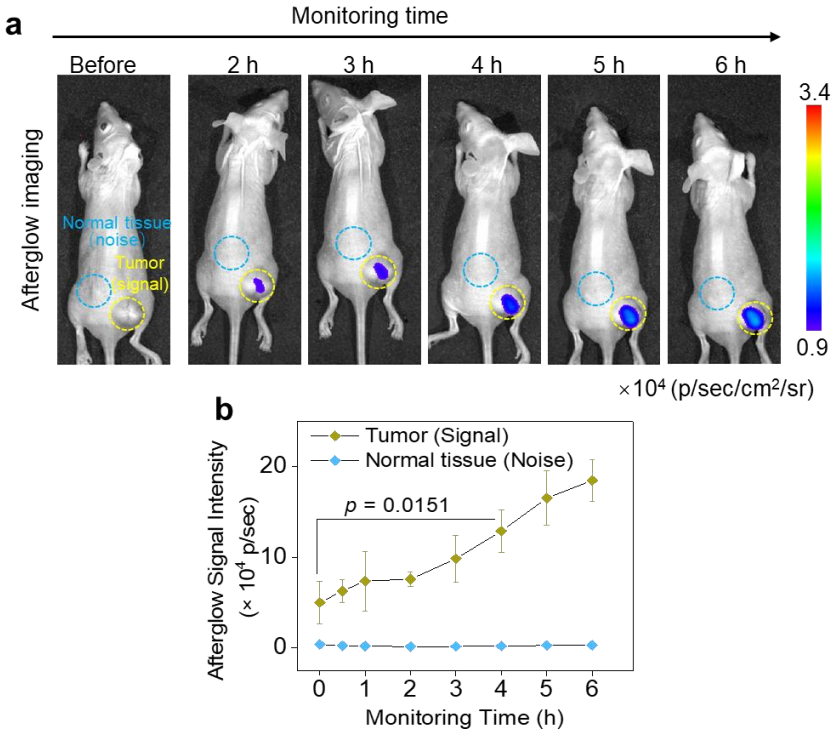

Supplementary Fig. 42 Afterglow imaging of mice after injection of APE1-probe (no targeting) (120 μL, 80 μg/mL) at different periods (10 mW/cm^2, irradiation time of 10 s, acquisition time of 60 s， n = 3 mice per group). (a) Afterglow images. (b) Quantified afterglow signal intensity. Data are presented as means ± SD. Statistical significance was determined using two-tailed Student's t-test for pairwise comparisons, and one-way ANOVA analysis of variance for multiple groups. P values > 0.05 were considered non-significant, while p values < 0.05 were considered statistically significant.

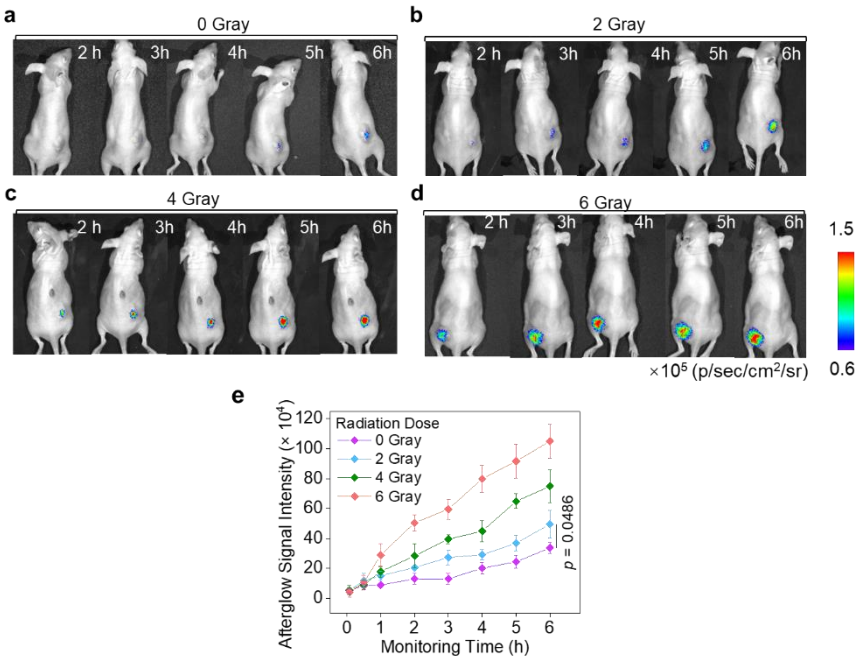

Supplementary Fig.43 Afterglow imaging of the mice treated with various radiation doses, and then intravenously injected with APE1-probe (120 μL, 80 μg/mL) (10 mW/cm^2, irradiation time: 10 s, acquisition time: 60 s, n = 3 mice per group). (a) 0 Gray radiation treatment. (b) 2 Gray radiation treatment. (c) 4 Gray radiation treatment. (d) 6 Gray radiation treatment. (e) Quantified afterglow signal intensity from (a – d). Data are presented as means ± SD. Statistical significance was determined using two-tailed Student's t-test for pairwise comparisons, and one-way ANOVA analysis of variance for multiple groups. P values > 0.05 were considered non-significant, while p values < 0.05 were considered statistically significant.

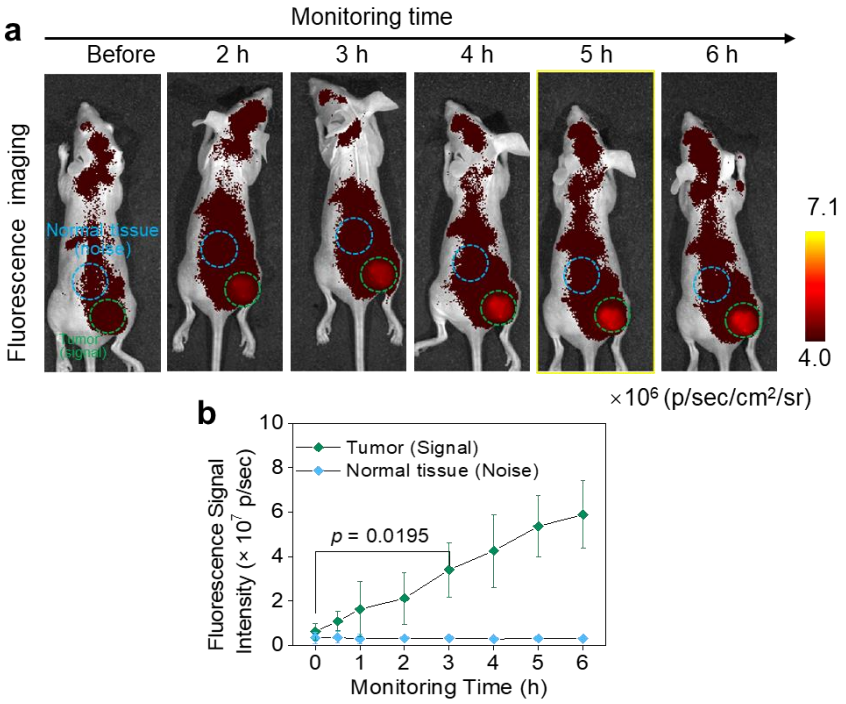

Supplementary Fig. 44 Fluorescence imaging of mice after injection of APE1-probe (no targeting) at different periods (Excitation wavelength: 605 nm, emission: Cy5.5 channel, n = 3 mice per group). (a) Fluorescence images. (b) Quantified fluorescence signal intensity. Data are presented as means ± SD. Statistical significance was determined using two-tailed Student's t-test for pairwise comparisons, and one-way ANOVA analysis of variance for multiple groups. P values > 0.05 were considered non-significant, while p values < 0.05 were considered statistically significant.

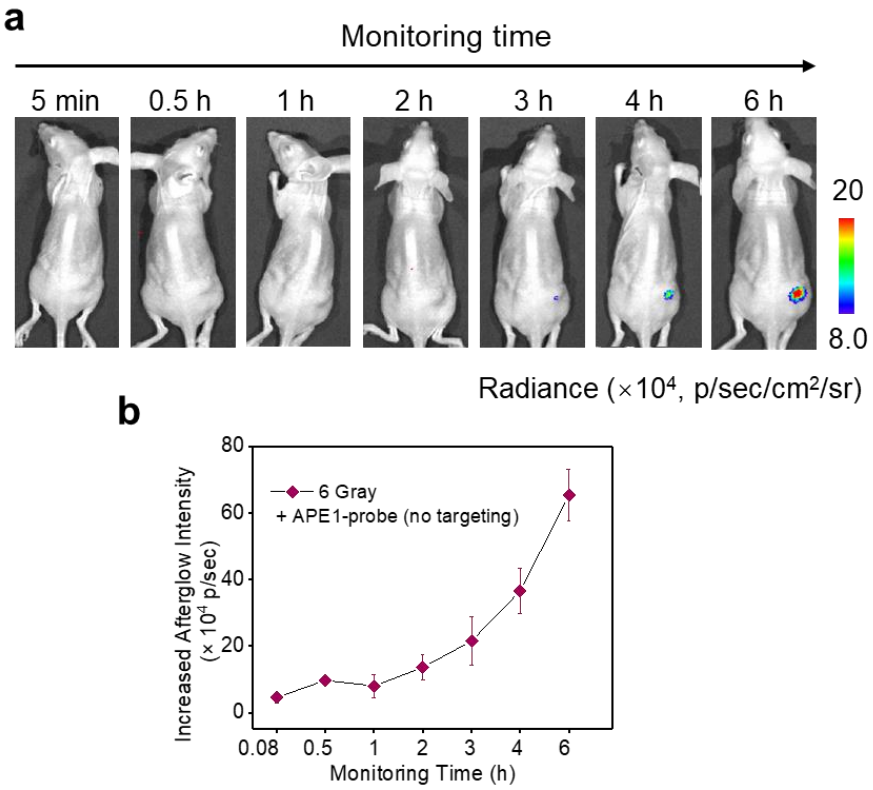

Supplementary Fig. 45 Afterglow imaging and quantification of signal intensity of the mice with the injection of APE1-probe (no targeting) after radiation treatment (6 Gray, 10 mW/cm^2, irradiation time: 10 s, acquisition time: 60 s, n = 3 mice per group). (a) Afterglow images. (b) Quantification of afterglow signal intensity from (a). Data are presented as means ± SD.

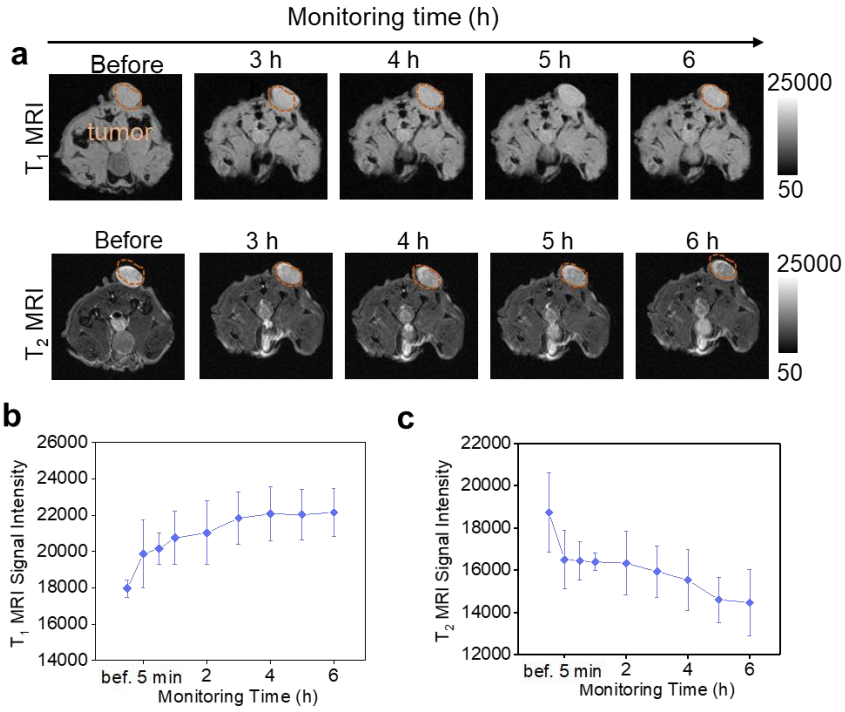

Supplementary Fig. 46 MRI imaging of the mice after intravenous injection of APE1-probe (no targeting) at different periods (n = 3 mice per group). (a) T_1 and T_2 MRI images. (b) Quantified T_1 MRI signal intensity. (c) Quantified T_2 MRI signal intensity. Data are presented as means ± SD.

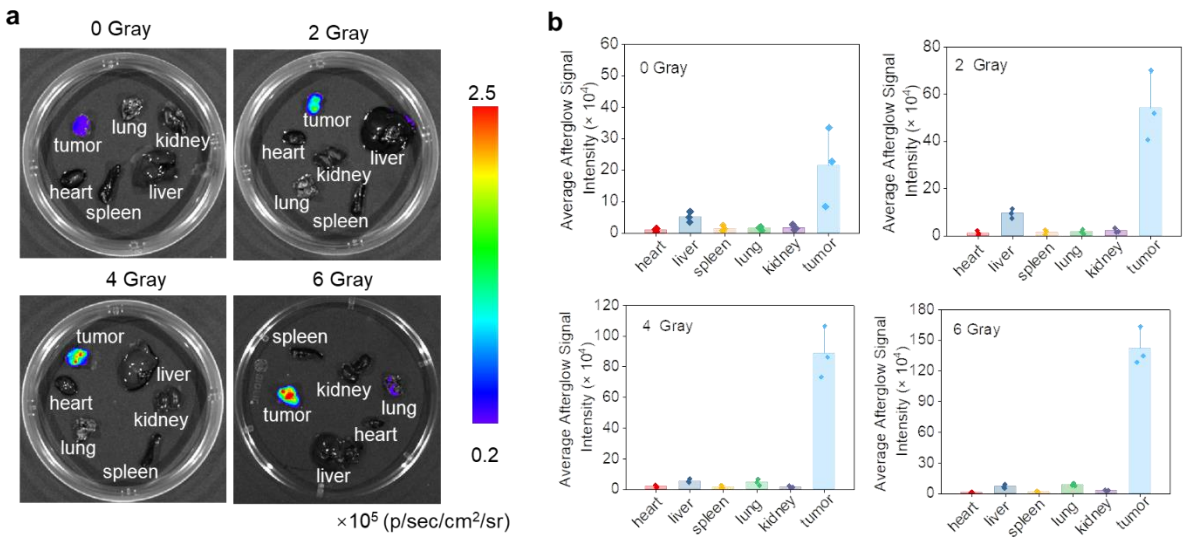

Supplementary Fig. 47 Afterglow imaging of organs and tumors harvested from mice at 8 hours post intravenous injection of APE1-probe (at 10-hour post-radiation treatment) (10 mW/cm^2, irradiation time: 10 s, acquisition time: 60 s, n = 3 mice per group). (a) Afterglow images. (b) Quantified afterglow signal intensity from (a). Data are presented as means ± SD.

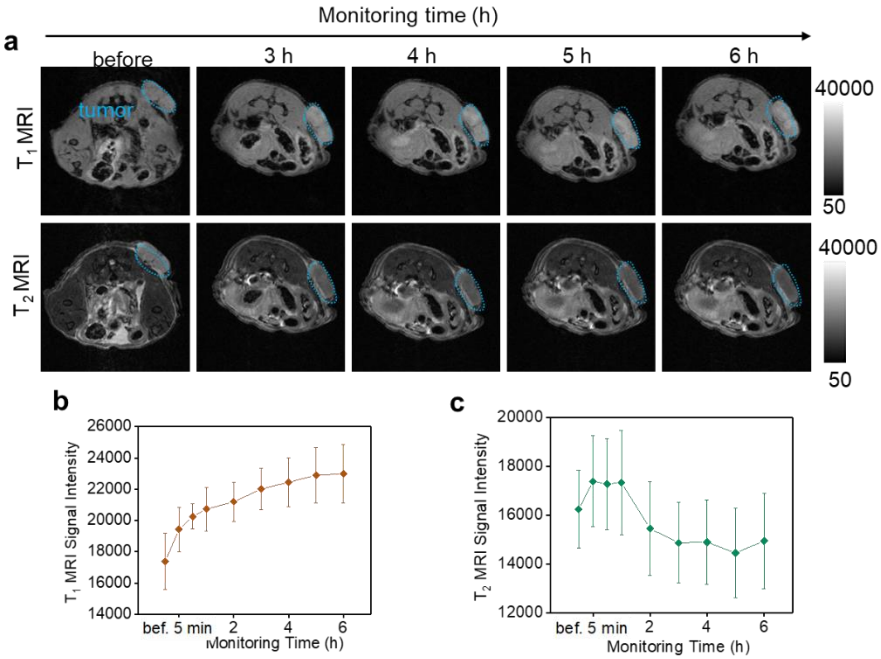

Supplementary Fig. 48 MRI imaging of the mice after intravenous injection of APE1-probe (n = 3 mice per group). (a) T_1 and T_2 MRI images. (b) Quantified T_1 MRI signal intensity. (c) Quantified T_2 MRI signal intensity. Data are presented as means ± SD.

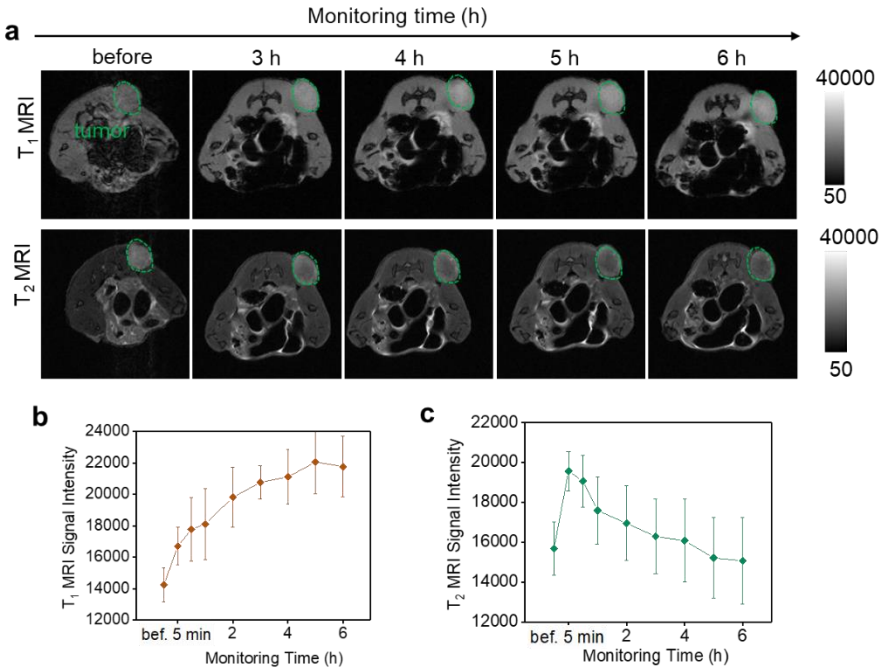

Supplementary Fig. 49 MRI imaging of the mice treated with 2 Gray radiation and then intravenous injection of APE1-probe (n = 3 mice per group). (a) T_1 and T_2 MRI images. (b) Quantified T_1 MRI signal intensity. (c) Quantified T_2 MRI signal intensity. Data are presented as means ± SD.

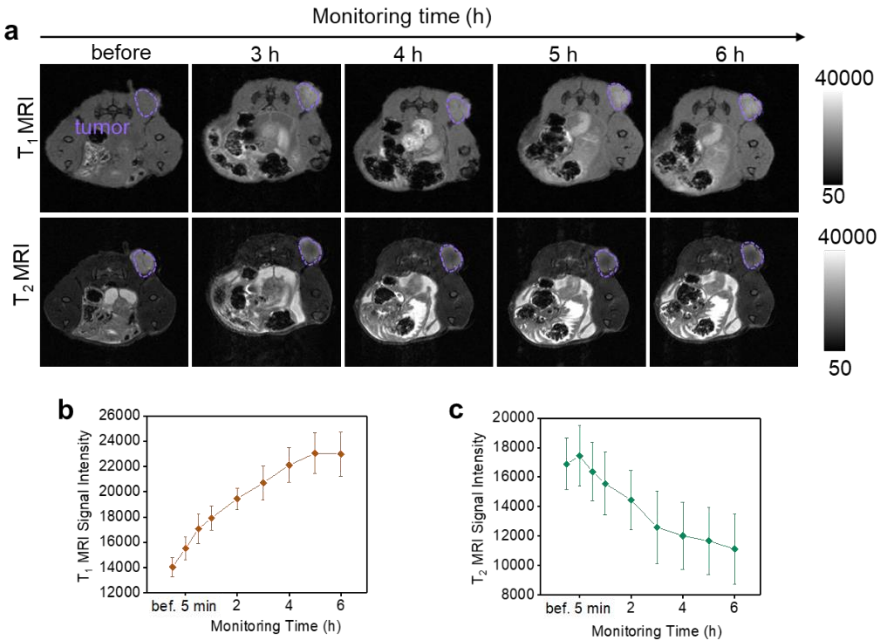

Supplementary Fig. 50 MRI imaging of the mice treated with 4 Gray radiation and then intravenous injection of APE1-probe (n = 3 mice per group). (a) T_1 and T_2 MRI images. (b) Quantified T_1 MRI signal intensity. (c) Quantified T_2 MRI signal intensity. Data are presented as means ± SD.

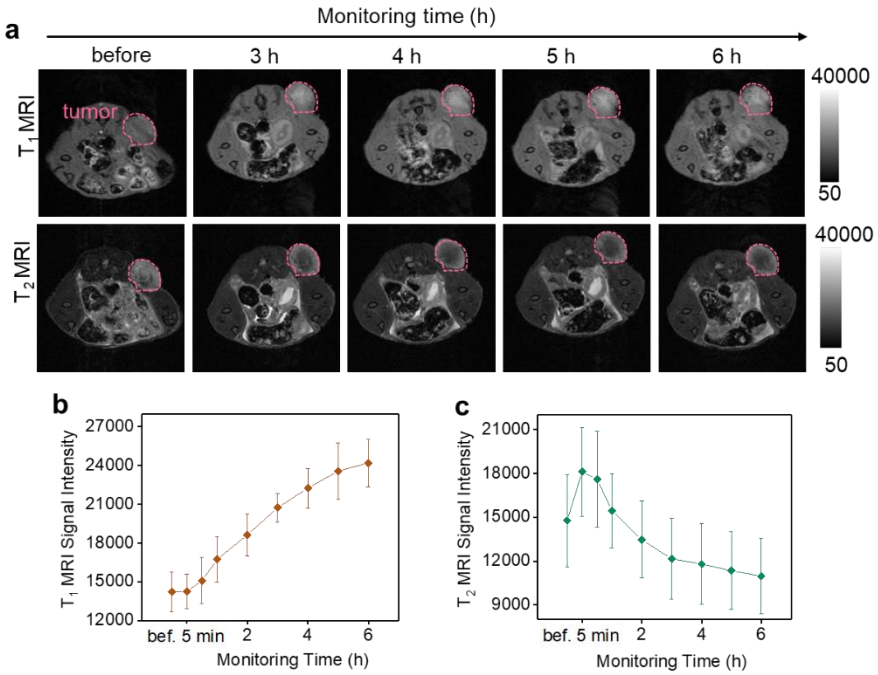

Supplementary Fig. 51 MRI imaging of the mice treated with 6 Gray radiation and then intravenous injection of APE1-probe (n = 3 mice per group). (a) T_1 and T_2 MRI images. (b) Quantified T_1 MRI signal intensity. (c) Quantified T_2 MRI signal intensity. Data are presented as means ± SD.

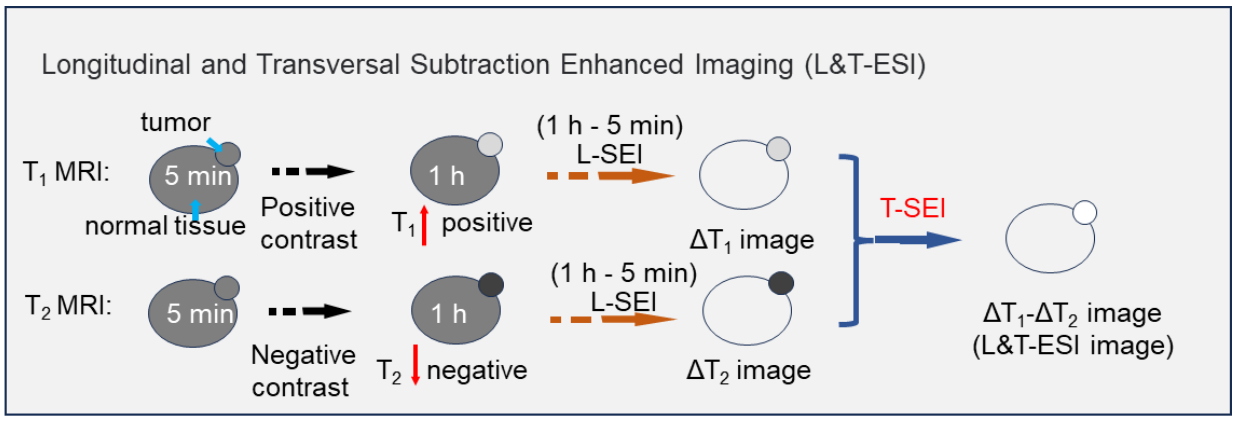

Supplementary Fig. 52 Subtraction process for longitudinal and transversal subtraction enhancd imaging (L&T-ESI).

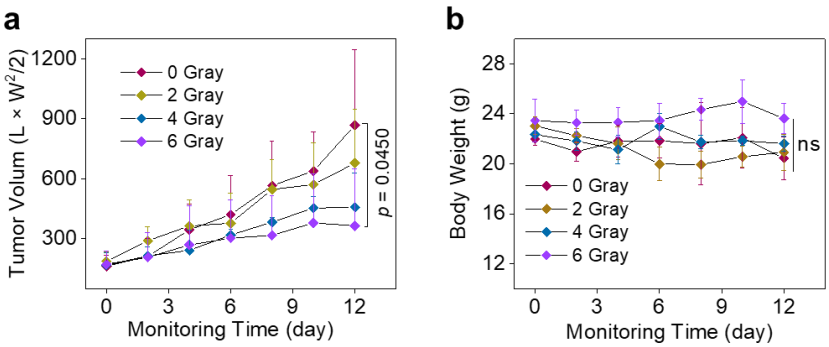

Supplementary Fig. 53 Radiotherapy for tumors of mice in vivo under various radiation intensities (n = 5 mice per group). (a) Tumor growth curve. (b) Body weight. Data are presented as means ± SD. Statistical significance was determined using two-tailed Student's t-test for pairwise comparisons, and one-way ANOVA analysis of variance for multiple groups. P values > 0.05 were considered non-significant (ns), while p values < 0.05 were considered statistically significant.

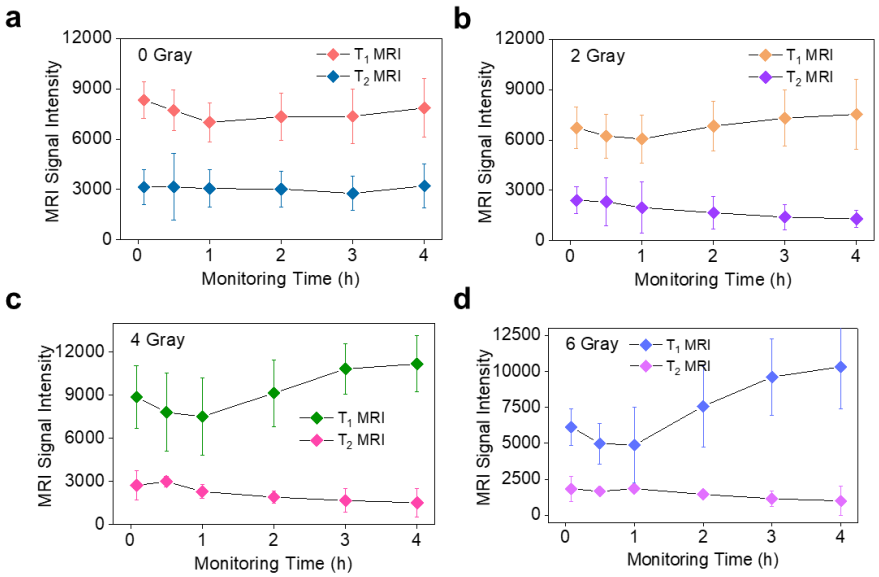

Supplementary Fig. 54 Quantified MRI signal intensity of the liver of mice after various radiation treatments and then intravenous injection of APE1-probe (n = 3 mice per group). (a) 0 Gray treatments. (b) 2 Gray treatments. (c) 4 Gray treatments. (d) 6 Gray treatments. Data are presented as means ± SD.

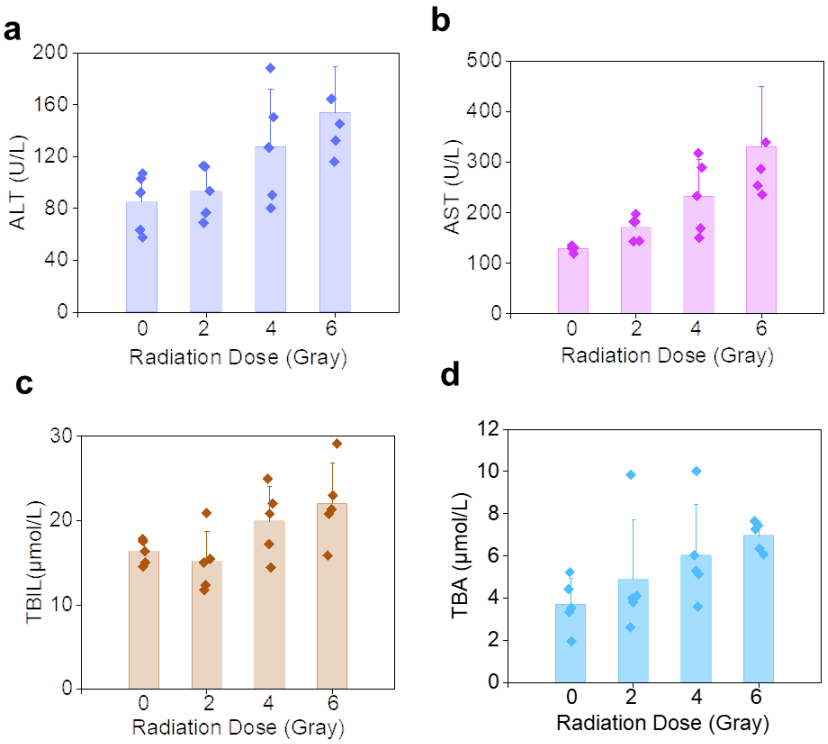

Supplementary Fig. 55 The determination of liver function index of the mice treated with various radiation doses (n = 5 mice per group). (a) Alanine aminotransferase (ALT), (b) Aspartate aminotransferase (AST), (c) Total bilirubin (TBIL), (d) Total bile acids (TBA). Data are presented as means ± SD.

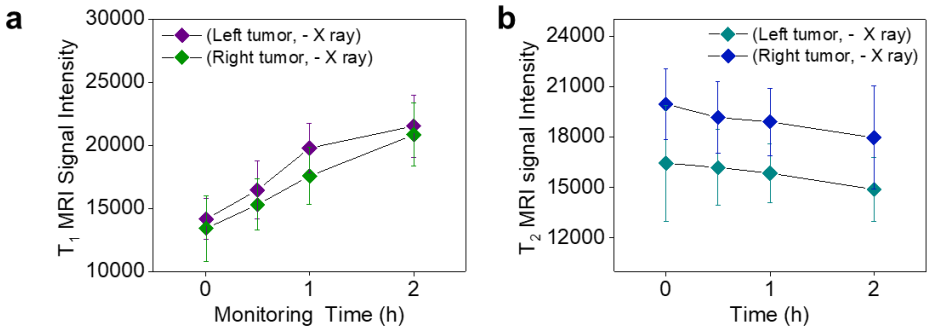

Supplementary Fig. 56 MRI signal intensity of the Group 2 mice with intravenous injection of APE1-probe (n = 3 mice per group). (a) T_1 MRI signal intensity. (b) T_2 MRI signal intensity. Data are presented as means ± SD.

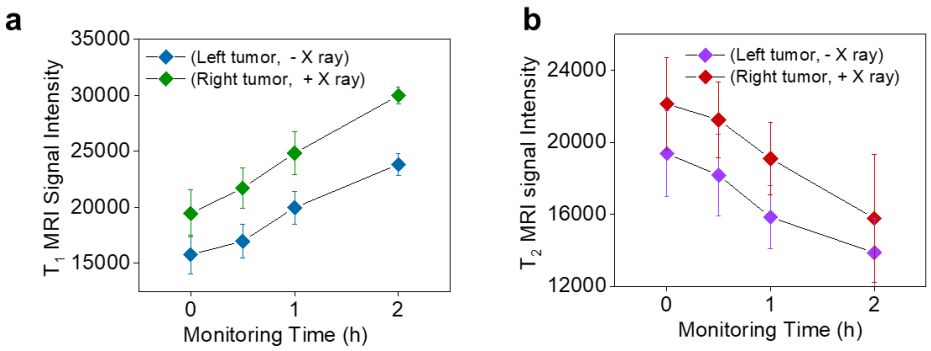

Supplementary Fig. 57 MRI signal intensity of the Group 1 mice with radiation treatment only in the right tumor and then intravenous injection of APE1-probe (n = 3 mice per group). (a) T_1 MRI signal intensity. (b) T_2 MRI signal intensity. Data are presented as means ± SD.

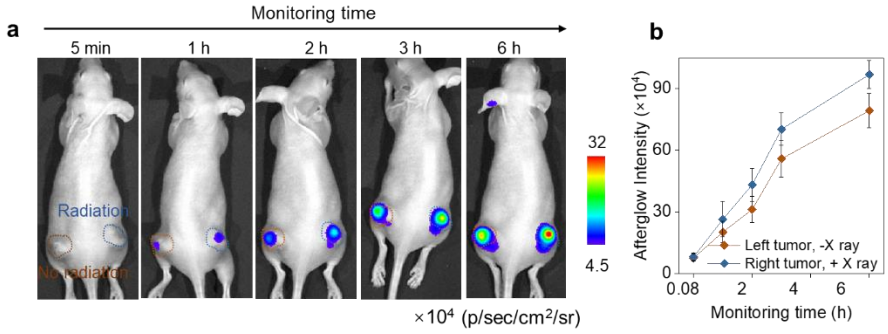

Supplementary Fig. 58 Afterglow imaging of the Group 1 mice with radiation treatment only in the right tumor and then intravenous injection of APE1-probe (10 mW/cm^2, irradiation time: 10 s, acquisition time: 60 s, n = 3 mice per group). (a) Afterglow images. (b) Quantification of afterglow signal intensity from (a). Data are presented as means ± SD.

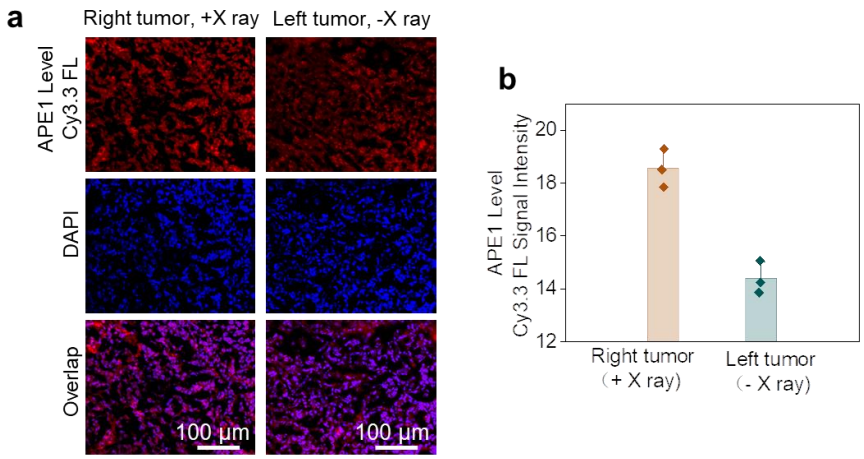

Supplementary Fig. 59 Fluorescence confocal images and signal intensity for immunofluorescence of tumors slice from the Group 1 mice with radiation treatment (6 Gray) only in the right tumor while no radiation by incubating with anti-APE antibody and Cy3-labeled IgG for testing APE1 level treatment in left tumor (n = 3 mice per group). (a) Fluorescence confocal images. (b) Mean fluorescence signal intensity. Data are presented as means ± SD.

Supplementary tables

No.	Detection method	Target	Imaging agent	In-vivo Imaging	Radiation types	Monitor therapy	Evaluate toxicity	Reference
1	Afterglow imaging MRI imaging	APE1	Afterglow nanoparticle $FeMnO_x$ nanoparticle	Yes	External beam radiation	Yes	Yes	This work
2	Immunohisto chemistry	Ki67	No	No (ex vivo tissue)	External beam radiation	No	No	*Histopathology*. 2023 Doi: 10.1111/his.15032.
3	PET	Chemokine receptor 4	^{68}Ga-pentixafor	Yes	Internal radioisotope radiation	No	No	*Clin. Nucl. Med.*,**42**, e29-e34 (2017).
4		Tumor accumulation	[^{68}Ga]PSMA-11	Yes	Internal radioisotope radiation	No	No	*Sci Rep.*,**11**,15263 (2021)
5	SPECT	Tumor accumulation	[^{123}I]NaI	Yes	Internal radioisotope radiation	No	No	*Mol. Pharmaceutics.*,**20**, 3460-3470 (2023)

Supplementary tab. 1 Representative companion diagnostic studies for guiding radiotherapy

Signal type	Limit of detection and medium	Design strategy	Detection range	In-vivo imaging	Background interference	Reference
Ultrastrong afterglow luminescence	0.0092 U/mL in 1× NeBuffer 4	No amplification	0 ~ 4 U/mL	Yes	No	This work
Subtraction-enhanced MRI	0.16 U/mL in 1× NeBuffer 4		0 ~ 2 U/mL			
Cy3 fluorescence	0.139 U/mL	No amplification	0 ~ 2.24 U/mL	No		*Chem. Sci.*, **10**, 5959–5966 (2019)
Cy5 fluorescence	3.34×10^{-5} U/mL In 1 × NEBuffer 4	DNA chain hybridization amplification	0 ~ 0.1 U/μL	No		*Chem. Sci*, **14**, 2318 (2023)
Cy5 fluorescence	0.23 U/mL in 1× NeBuffer 4	No amplification	0.5 ~ 100 U/mL	No		*Anal. Chem.*, **95**, 3551−3555 (2023)
FAM fluorescence	0.007 U/ mL unmentioned medium	Toehold-mediated strand displacement	0 ~1 U/mL	No		*Angew. Chem. Int. Ed.*, **62**, e202213884 (2023)
Cy5 fluorescence	0.01 U/mL in 1×Nebuffer 1.1	Catalytic hairpin assembly	0.2 ~1 U/mL	No		*Chem. Sci.*, **11**, 10361–10366 (2020)
FAM and TAMRA fluorescence	7.8×10^{-5} U/ mL in buffer	Hybridization chain reaction and catalytic hairpin assembly	0.0001 ~ 1.0 U/ mL	No		*Small*, **19**, 2207736 (2023)
Cy5.5 fluorescence	0.22 U/mL in 1× NeBuffer 4	No amplification	0 ~ 2 U/mL	Yes	Autofluorescence	ACS Nano, **14**, 13792−13810 (2023)
Cy3 fluorescence	0.078 U/mL in Tris-acetate buffer	No amplification	0 ~ 1 U/mL	Yes	Autofluorescence	ACS Appl. Mater. Interfaces **15**, 22, 26316–26327 (2023)
Cy5 fluorescence	0.01 U/mL In Tris-HCl buffer	No amplification	0 ~ 0.1 U/mL	Yes	Autofluorescence	Angew. Chem. Int. Ed. **60**,14887 -14891 (2021)

Supplementary tab. 2 Characterization comparison of the representative probe for APE1 detection.

Organic afterglow particle	Excitation source	Minimum excitation powder density in solution	Maximum emission wavelength or range	Emission lifetime	Afterglow intensity in solution and in vivo imaging of subcutaneous tumor	References
TA NPs	White light source	60 μW/cm^2	640 nm	$t_{1/2}$ ≈600 s	In 1×NeBuffer: ~1.6× 10^6 (p/s/cm^2 /sr)/(5 μg/mL) with white light irradiation (10 mW/cm^2) of 10 s and acquisition time of 60 s; In vivo imaging: ~1× 10^6 (p/s/cm^2 /sr)/(80 μg/mL, 120 μL) with white light irradiation (10 mW/cm^2) of 10 s and acquisition time of 60 s	This work
P1–P5 polymers	365 nm UV light	20 mW/cm^2	508 nm	$t_{1/2}$ ≈869 ms	None	*J. Am. Chem. Soc.* **2023**, 145, 13, 7343–7351
MAS-pH/AL/Cu/GSH	660 nm laser	0.5-1.0 W/cm^2	510-570 nm	$t_{1/2}$ ≈30 s	In PBS buffer: ~8× 10^5 (p/s/cm^2/sr)/(50 μg/mL) with 660 nm laser irradiation (0.5 W/cm^2) of 30 s, and acquisition time of 10 s; In vivo imaging: ~ 10^4 (p/s/cm^2/sr)/(100 μg/mL, 25 μL) with 660 nm laser irradiation (1.0 W/cm^2) of 30 s, and acquisition time of 30 s	*J. Am. Chem. Soc.* **2023**, 145, 24386-24400
MAP-pH /$O_2^{\bullet-}$ /LAP	660 nm laser	0.8-1.0 W/cm^2	510-570 nm	$t_{1/2}$ ≈60 s	In PBS buffer: ~2-6× 10^5 (p/s/cm^2/sr)/(50 μg/mL) with 660 nm laser irradiation (0.8 W/cm^2) of 30 s and acquisition time of 30 s; In vivo imaging: ~4 ×10^5 (p/s/cm^2/sr)/((50 μg/mL, 25 μL) with a 660 nm laser irradiation (1.0 W/cm^2) of 30 s and acquisition time of 30 s	*J. Am. Chem. Soc.* **2023**, 145, 9, 5134–5144
Chlorin Nanoparticle	Halogen lamp, 808 nm laser	0.1 W/cm^2 or 1 W/cm^2	660-680 nm	$t_{1/2}$ ≈1.5 h	In PBS buffer: ~1.5 × 10^6 (p/s/cm^2/sr)/(50 μM) with Halogen lamp irradiation of 60 s and acquisition time of 10 s; In vivo imaging:~3×10^3 (p/s/cm^2/sr)/(25 μg/mL, 50 μL) with Halogen lamp irradiation of 60 s and acquisition time of 10 s.	*J. Am. Chem. Soc.* **2022**, 144, 15, 6719
P-TNP	White LED lamp, xenon lamp	2 W/ cm^2	630 nm	$t_{1/2}$ ≈120 s	In H_2O solution: ~800 (cps/mm^2)/(100 mg/mL) with white LED lamp irradiation (2 W/cm^2) of 60 s, and acquisition time of 60 s; In vivo imaging:~1.5×10^4 (p/s/cm^2/sr)/(0.1 mg/mL, 200 μL) with white LED lamp irradiation (2 W/cm^2) of 120 s, and acquisition time of 60 s	*Chem. Sci.*,**2020**, 11, 419
$F1^{2+\bullet}$-ANP	808 nm laser	1 W/cm^2	775 nm	$t_{1/2}$ ≈396 s	In PBS buffer: ~6×10^6 (p/s/cm^2/sr)/(58/28/2.2 μg/mL F12*$(BF^{4-})_2$/MEH-PPV/NIR775) with 808 nm laser irradiation (1W/cm^2) of 60 s, and acquisition time of 60 s; In vivo imaging: ~3×10^5 (p/s/cm^2/sr)/(211/100/8 μg F12*$(BF^{4-})_2$/MEH-PPV/NIR775, 200 μL) with 808 nm laser irradiation (1W/cm^2) of 60 s, and acquisition time of 60 s.	*Nat. Commun.*,**2020**, 11, 446
OSN1-T	365 nm UV light	10 mW/cm^2	530 nm and 570 nm	$t_{1/2}$ ≈10s	In PBS buffer: ~6×10^{10} (p/s/cm^2/sr)/(1.6 μM) with handheld UV lamp irradiation (12 W) of 60 s, and acquisition time of 10 s; In vivo imaging:~1.5×10^4 (p/s/cm^2/sr)/(16 μM)with UV light irradiation (18 mW/cm^2) of 60 s, and acquisition time of 10 s	*Adv. Mater.* **2017,** 29, 1606665
SPN-NCBS; SPN-thiol	808 nm laser	1 W/cm^2	780 nm	$t_{1/2}$ ≈396 s	In water: ~1×10^6 (p/s/cm^2/sr)/(1.25 μg/mL) with 808 nm laser irradiation (1 W/cm^2) of 60 s, and acquisition time of 30 s; In vivo imaging:~5.7×10^5 (p/s/cm^2/sr)/(μg/mL), 0.25 mg/mL, 2 μL) with 808 nm laser irradiation (0.5 W/cm^2) of 60 s, and acquisition time of 180 s	*Nat. Biotechnol.* **2017**, 35, 1102-1110
APtN	808 nm laser	0.25 W/cm^2	550 nm	$t_{1/2}$ ≈960 s	In PBS buffer: ~1.5×10^6 (p/s/cm^2/sr)/(1 mg/mL) with 808 nm laser irradiation (0.25 W/cm^2) of 10 s, and acquisition time of 60 s; In vivo imaging:~1.5×10^4 (p/s/cm^2/sr)/(400 μg/mL, 200 μL) with 808 nm laser irradiation (0.25 W/cm^2) of 20 s, and acquisition time of 60 s	*Adv. Mater.* **2019,** 31, 1902672
mTPA-N	365 nm UV light	95 mW/cm^2	515 – 640 nm	$t_{1/2}$ ≈13 ms	In aqueous solution: ~7×10^4 (p/s/cm^2/sr)/(300 μg/mL) with UV irradiation (95 mW/cm^2) of 5 s and exposure time of 5 s; In vivo imaging:~9×10^5 (p/s/cm^2/sr)/(600 μg/mL, 50 μL) with UV irradiation (95 mW/cm^2) of 5 s, and exposure time of 5 s	*Adv. Mater.* **2020,** 32, 2006752
Q-SNAP	Ultrasound	1.5 W/cm^2	780 nm	$t_{1/2}$ ≈ 90 s	In PBS buffer:~2×10^6 (p/s/cm^2/sr)/(10 μg/mL) with ultrasound irradiation (1.5 W/cm^2) of 30 s, and acquisition time of 1 s; In vivo imaging: ~7×10^4 (p/s/cm^2/sr)/(2 mg/kg mice) with ultrasound irradiation (1.5 W/cm^2) of 30 s and acquisition time of 10 s	*Adv. Mater.* **2023**, *35*, 2211651
TPP-DO	Halogen lamp	50 mW/cm^2	650 nm	$t_{1/2}$ ≈120 s	In PBS buffer:~4.0×10^8 (p/s/cm^2/sr)/(25 μM) with halogen lamp irradiation (50 mW/cm^2) of 10 s, and acquisition time of 5 s; In vivo imaging: ~4.0×10^6 (p/s/cm^2/sr)/(200 μg/mL, 200 μL) with halogen lamp irradiation (50 mW/cm^2) of 10 s, and acquisition time of 10 s for;	*Angew. Chem. Int. Ed.* **2024,** 63, e202313117

Supplementary tab. 3 Luminescence characterization comparison of reported organic afterglow materials.

Supplementary References

1. Li, Y. *et al.* Bay- and ortho-octa substituted perylenes. *Org. Lett.* **19**, 5094-5097 (2017).
2. Guo, J. *et al.* Large aromatic hydrocarbon radical cation with global aromaticity and state-associated magnetic activity. *Chem. Mater.* **32**, 5927-5936 (2020).